Infocommunications Journal

A PUBLICATION OF THE SCIENTIFIC ASSOCIATION FOR INFOCOMMUNICATIONS (HTE)

September 2016 Volume VIII Number 3 ISSN 2061-2079

Technically Co-Sponsored by

IEEE ComSoc™ IEEE Communications Society

hte

IEEE HUNGARY SECTION

Indexing information

Infocommunications Journal is covered by Inspec, Compendex and Scopus.
Infocommunications Journal is also included in the Thomson Reuters – Web of ScienceTM Core Collection, Emerging Sources Citation Index (ESCI)

Infocommunications Journal

Technically co-sponsored by IEEE Communications Society and IEEE Hungary Section

Supporters

FERENC VÁGUJHELYI – president, National Council for Telecommunications and Information Technology (NHIT)
GÁBOR MAGYAR – president, Scientic Association for Infocommunications (HTE)

Editorial Office (Subscription and Advertisements)**:**
Scientic Association for Infocommunications
H-1051 Budapest, Bajcsy-Zsilinszky str. 12, Room: 502
Phone: +36 1 353 1027
E-mail: info@hte.hu • Web: www.hte.hu

Articles can be sent also to the following address:
Budapest University of Technology and Economics
Department of Telecommunications and Media Informatics
Tel.: +36 1 463 1102, Fax: +36 1 463 1763
E-mail: vida@tmit.bme.hu

Subscription rates for foreign subscribers: 4 issues 10.000 HUF + postage

Publisher: PÉTER NAGY

HU ISSN 2061-2079 • Layout: PLAZMA DS • Printed by: FOM Media

Non-orthogonal Frequency Hopping Signal Underdetermined Blind Source Separation in Time-Frequency Domain

[1] Chengjie Li [1] Lidong Zhu [2] Zhen Zhang

***Abstract*—In this paper, a novel Matching Optimization Algorithm (MOA-algorithm) based on underdetermined blind source separation is proposed for non-orthogonal frequency hopping signal (that is, inner products are not always equal to zero in the same time-frequency point). Compared to traditional methods, the separation method is formulated as matching optimization. In our method, we accomplish the underdetermined blind source separation by computing the Short Time Fourier Transform (STFT) of each observation to get the signal time-frequency distribution, then we formulate the separation problem as matching optimization. In matching optimization, a new cost function is designed to improve the complete separation, and we make negative gradient direction as the steepest descent direction, to verify the proposed method on several simulations. The experimental results demonstrate the effectiveness of the proposed method.**

***Index Terms*—Blind Source Separation, Frequency hopping signal, Time-Frequency Distribution, Cost Function, Pearsons correlation coefficient.**

1 2 3

I. INTRODUCTION

Blind source separation (BSS) is a major research area in signal processing and machine learning, and is used in many fields, such as image recognition, speech enhancement, biomedical signal processing, wireless communications etc. [1][2][3]. BSS aims to extract individual components from their mixture samples where there is very limited, or no, prior information on mixture samples or the mixing process. Recently, many BSS methods are based on Independent Component Analysis with the assumption that the sources are independent signals. Some other methods based on Wigner-Ville Distribution (WVD) are proposed, but there is a contradiction between time-frequency concentration and cross-term interference in these methods [4]. At present, most traditional BSS methods assume that the source signals are statistically independent or the mixed matrix is full column rank. However, in many situations, this hypothesis is not valid. Consequently, recovering the source signals by multiplying the mixed matrix's pseudo inverse cannot be used. In practical terms, the overdetermined mixture assumption is not always satisfied, thus it is necessary to solve the problem of underdetermined blind source separation (UBSS). Compared with the classical BSS approaches, the method in this article requires less constraints on the source signals, such as stationarity and independence. So it is more suitable to separate non-stationary sources, such as Frequency-Hopping (FH) signal.

Frequency-Hopping (FH) signal has been widely used in military field and modern communication systems due to its high security and good anti-jamming ability [5]. To meet the need of Counter-reconnaissance, FH signal blind source separation research has been a focus. Recently, some researchers discuss orthogonal FH signals underdetermined blind source separation method based on sparsity [6][7], however, non-orthogonal Frequency Hopping Signal Underdetermined Blind Source Separation is a challenge. In this article, we propose a non-orthogonal underdetermined blind source separation method based on convex optimization methods, that is, MOA-algorithm. The problem is described as follows: (a) By computing the Short Time Fourier Transform (STFT) of each observation, we can get the signal' time-frequency distribution. (b) We construct the cost function according to the sample data in time-frequency domain. (c) We find the optimal solution of the cost function by using the steepest descent method.

The rest of this paper is organized as follows. In Section II, we introduce the preparatory work of this article, In Section III, we introduce the blind source signal separation algorithm, that is, MOA-algorithm. In Section IV, we introduce and discuss the experimental results. Finally, the conclusion is drawn in Section V.

II. PREPARATORY WORK

In this section, we introduce the related preparatory work of MOA-algorithm.

A. BSS Model

BSS aims at separating a set of N unknown sources from a set of M observations. Usually, the observations are obtained from M sensors, each sensor receives a mixture from those sources, the framework of BSS model is as below:

The principle of BSS is shown in Fig.1. The matrix $S(t) = [s_1(t), s_2(t), \cdots, s_N(t)]$ is composed of N unknown sources, and the matrix $Y(t) = [y_1(t), y_2(t), \cdots, y_M(t)]^T$ represents M observations. Considering linear instantaneous mixtures model only, each observation is described as below [8]:

$$y_j(t) = \sum_{i=1}^{N} a_{ij} s_j(t) + n_i(t), j = 1, 2, \cdots, M \qquad (1)$$

[1]University of Electronic Science and Technology of China, Chengdu, Sichuan, China, E-mail: junhongabc@126.com, zld@uestc.edu.cn

[2]NCS Pte. Ltd. of Singapore Tele-communications Limited, Ang Mo Kio Street 62, NCS Hub, Singapore, E-mail: zhangzhen@ncsi.com.cn

[3]Manuscript submitted on August 29, 2016

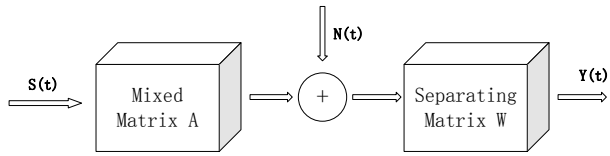

Fig. 1. Framework of BSS Model

here, a_{ij} is the (i,j)th element of the mixed matrix, $n_i(t)$ is the ith component of the noise. Equation (2) can also be written in matrix form,

$$Y(t) = AS(t) + N(t) \tag{2}$$

According to the relationships among the numbers of original signal (M) and the numbers of receiving antenna(N), blind source signals can be classified into overdetermined blind separation ($M < N$), determined blind separation ($M = N$) and underdetermined blind separation ($M > N$).

B. Frequency-Hop Signal Model

The FH signal is a kind of non-stationary signals whose carrier frequency changes along with time, it can be expressed as [5]:

$$\begin{aligned} f(t) = \sqrt{2S}\sum_{k} rect_{T_H}(t - kT_H - \alpha T_H) \\ \cdot e^{j2\pi f_k(t-kT_H-\alpha T_H)+j\theta} + n(t), 0 < t \le L \end{aligned} \tag{3}$$

here, L is the length of the sample data, $rect_{T_H}$ is the rectangular window whose width equals to T_H, T_H is the hop duration, f_k is the carrier frequency of the kth hop, αT_H is hop timing, θ is the phase of the Fh signal, $n(t)$ is additive noise, S is the power of the signal.

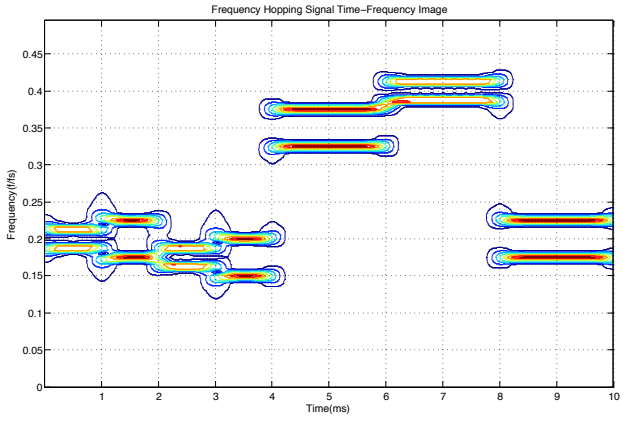

Fig. 2. Frequency Hopping Signal Time-Frequency Image

Fig.2 describes the time-frequency distribution of a FH signal. we can see there are five hops in this sample. The length of the whole hops is one hop duration. We can see that all hops of the FH signal are actually finite sine waveforms without any overlap in time domain with each other. Each of the finite sine waveforms is uniquely decided by the three followed parameters, T_k denotes the location of kth hop in time domain, f_k denotes the location of kth hop in frequency domain, T_H denotes the length in time domain.

The problem in this paper focuses on how to separate the initial Non-orthogonal Frequency Hopping Signal without any more prior knowledge.

III. MOA-ALGORITHM

A. Problem Formulation

The mixed signals are certain to collide in the time-frequency domain when the mixed signals are non-orthogonal, as is shown in Fig.3. We can judge whether signals collide according to the number of signals in frequency domain [9]. The signals do not collide if the signal number is equal to the number of source signals in frequency domain. The signals collide if the signal number is less than the number of source signals in frequency domain. We can separate the mixed signals with Density Component Analysis Method when the source signals do not collide [10], which will be concisely introduced in the following part 3.2, and the separated signal will be signal vector space $\mathscr{Y}_1$. The mixed collided source signals will be the mixed signal vector space $\mathscr{Y}_2$. We can separate them with Matching Optimization Algorithm (MOA).

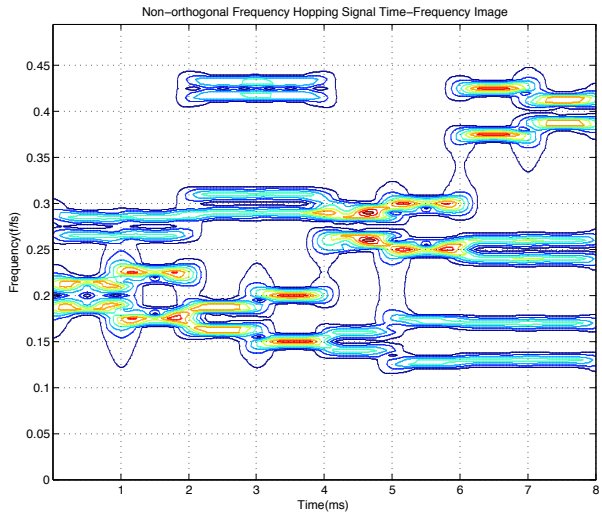

Fig. 3. Non-orthogonal Frequency Hopping Signal Time-Frequency Image

B. Density Component Analysis Method

In this section, we introduce the Density Component Analysis Method concisely, and the detailed research is another research.

(1) Construct Cost Function Pair (ρ_i, δ_i)

According to the time-frequency domain sampling points i, we compute two quantities: its local density ρ_i and its distance δ_i from points of higher density. Both quantities depend only on the distances d_{ij} between sampling data points, which are assumed to satisfy the triangular inequality. The local density ρ_i of data point i is defined as:

$$\rho_i = \sum_j \chi(d_{ij} - d_c) \tag{4}$$

in above equation, if $x < 0$ then $\chi(x) = 0$ otherwise $\chi(x) = 1$, d_c is a cutoff distance. Basically, ρ_i is the number of sampling points, the distance of sampling points to sampling point i is smaller than d_c. The algorithm is sensitive only to the relative magnitude of ρ_i in different points, that is to say, for large data sets, the results of the analysis are robust with respect to the choice of d_c.

δ_i is measured by computing the minimum distance between the sampling point i and any other sampling point with higher density:

$$\delta_i = min_{j:\rho_j > \rho_i}(d_{ij}) \tag{5}$$

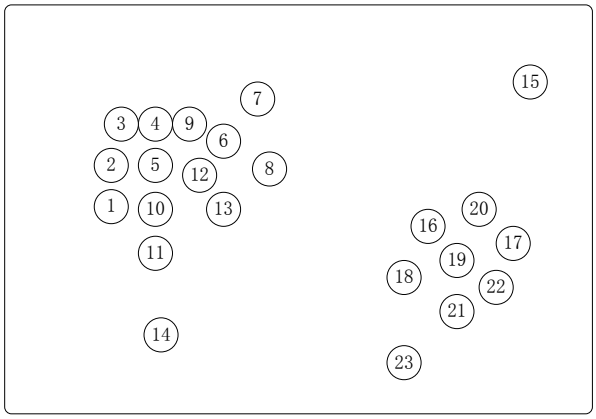

Fig. 4. Decision Coordinate System. Sampling Data Points are Ranked in Order of Decreasing Density

(2) Construct Decision Coordinate System

This observation, which is the core of the algorithm, is illustrated by the simple example in Fig.4. Fig.4 shows 23 points embedded in a two-dimensional space [25]. Based on

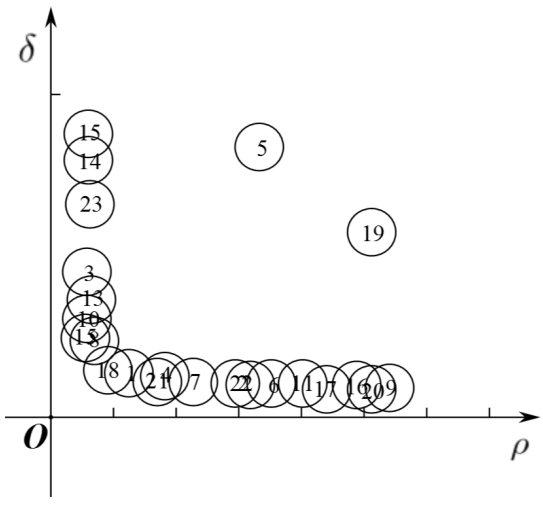

Fig. 5. Decision Coordinate System. Sampling Data Points are Ranked in Order of Decreasing Density

the distribution of the sampling points in a two-dimensional space above, decision coordinate system can be found in Fig.5, which shows the plot of δ_i as a function of ρ_i for each sampling point. It is seen that although the data number 2 and 22 are very near, they are not the cluster center due to the small value of δ. Meanwhile, we can see from Fig.5 that data 2 and 22 belong to different centers, i.e., 5 and 19 respectively. Hence, only the data with both large values of δ and ρ will be treated as cluster center, such as data number 5 and 19 in Fig.5. Note that the points 14, 15, and 23 have a relatively high δ and a low ρ. These points are isolated data and can be considered as clusters with single point, which is also named outliers.

After the cluster centers have been found, each remaining sampling point is assigned to the same cluster as its nearest neighbor of higher density.

We can separate the mixed signals with the above Density Component Analysis Method when the source signals do not collide, and the separated signal will be signal vector space $\mathscr{Y}_1$. The mixed collided source signals will be the mixed signal vector space $\mathscr{Y}_2$. We can separate the mixed signal vector space $\mathscr{Y}_2$ with MOA-algorithm as follows.

C. Construct Cost Function of MOA-algorithm

According to the separated signal vector space $\mathscr{Y}_1$ and the mixed collision source signals vector space $\mathscr{Y}_2$, we can construct the following cost function.

$$\min_{A,E} \| \beta - \sum \lambda_i x_i \|_p + E, \quad subject\ to\ x_i \in X \tag{6}$$

here, β is the collision vector, and belongs to the $\mathscr{Y}_2$. λ_i is the weight coefficient of x_i. $\sum x_i$ is the random sum of x_1, x_2, $\cdots$, x_n, $x_i \in \mathscr{Y}_1$. $A = [x_i, x_(i+1), x_(i+2), \cdots, x_(i+k)]$. E is the Mean Squared Error(MSE), here,

$$E = \sqrt{\frac{\sigma_1^2 + \sigma_2^2 + \cdots + \sigma_n^2}{n}}, \tag{7}$$

σ_1, σ_2, $\cdots$, σ_n is the error value.

We find the optimal solution of the cost function by using the steepest descent method. So, the negative gradient direction $d = -\frac{\nabla min(\cdot)}{\|\nabla min(\cdot)\|}$ is the steepest descent direction [11].

IV. PERFORMANCE ANALYSIS OF MOA-ALGORITHM

A. Algorithm Process Analysis

MOA-algorithm aims at reconstructing the mixed matrix and the source signal according to $\mathscr{Y}_1$, $\mathscr{Y}_2$ by solving the following optimization problem:

$$\min_{A,E} \| \beta - \sum \lambda_i x_i \|_p + \sqrt{\frac{\sigma_1^2 + \sigma_2^2 + \cdots + \sigma_n^2}{n}}, \quad subject\ to\ x_i \in X \tag{8}$$

where the first term penalizes non-sparse solutions, the last term is a classical data fidelity term. Because $\mathscr{Y}_1$ is separated signal vector space, it is sparse. The sparsity level is measured by the l_p norm of the sources. We generally choose either $p = 1$ or $p = 2$. In [12], [13], how to choose to a particular l_p norm for the sparsity penalty have been discussed in more

detail. If E is fixed, the l_2 norm is particularly appealing since it makes the estimation of β be a convex optimization problem. In MOA-algorithm, we will choose $p = 2$ which has been shown to provide the best separation results in the following simulations in part 5. So, the problem in (8) is classically tackled by using the steepest descent method. So, the negative gradient direction $d = -\frac{\nabla min(\cdot)}{\|\nabla min(\cdot)\|}$ is the steepest descent direction.

According to (8), the mixed matrix A is estimated by looking for the optimal solution of the following convex problem:

$$\min_{A} \| \beta - \sum \lambda_i x_i \|_p + E, \quad subject\ to\ x_i \in X \tag{9}$$

The equation (9) can be decomposed into two terms: i) a non-convex $p-norm$ penalty, and ii) a quadratic and differentiable data fidelity term E. Let $\forall x_1, x_2 \in \mathscr{Y}_1$, $\mid E(x_1) - E(x_2) \mid \leq L \mid x_1 - x_2 \mid$, the quadratic term E is differentiable and its gradient satisfied $L - Lipschitz$ conditions. That shows the problem in (9) can be solved exactly by using the Forward-Backward splitting algorithm [14]. In [15], this optimization strategy has been used for solving the steepest descent method, but it has the strong weakness of dramatically increasing the computational cost of the algorithm: update A would require efficient but costly iterative algorithms. Furthermore, each time the source matrix A is updated in the algorithm MOA algorithm, it is fully re-estimated. Therefore, it may not be necessary to update with high precision A at each step of MOA algorithm.

B. Convergence of MOA-Algorithm

Because the problem in (8) is not convex, convergence to a critical point can be expected. For a fixed collision vector β (β belongs to the $\mathscr{Y}_2$), minimizing the problem in (8) can be tackled by Block Coordinate Relaxation [16]. Then, this procedure can make solve sequences of convex minimization problems take place of a globally non-convex problem. In [17], convergence of block coordinate relaxation for the minimization of non-differentiable and non-convex cost functions have been proved by Tseng. According to [17], the minimization of function in (8) converges to a critical point when the parameters λ_i and x_j are fixed .

Firstly, decreasing the thresholds is a strategy to improve the robustness of the MOA algorithm to spurious local minima. In the field of optimization, this procedure is reminiscent of the fixed point continuation technique, which has been proposed to speed up the minimization of $\| \bullet \|_p$-penalized least-squares [18]. The convergence of the MOA algorithm would be guaranteed as long as steps (8) are alternated until convergence for each value of λ_i. The thresholds are however updated at each iteration of the MOA algorithm, which helps speeding up the algorithm but might prevent it from convergence.

Secondly, weight coefficient λ_i is updated at each iteration, but also might prevent the MOA algorithm from convergence. Lastly, in the spirit of re-weighted l_1 techniques, the weight coefficients are updated based on estimating of $x_j \in \mathscr{Y}_2$ [49 19]. If this strategy is a well motivated heuristic, the convergence of the MOA algorithm is not theoretically grounded.

In numerical experiments, in order to show better performance of the proposed algorithm, we measure the convergence speed with E_{ct} value. The results are shown in Fig.6, the horizontal axis is iteration number, the vertical axis is E_{ct} value and E_{ct} is defined as [20]:

$$E_{ct} = \sum_{i=1}^{M}(\sum_{j=1}^{M}) \frac{\mid c_{ij} \mid}{max_k \mid c_{ik} \mid -1} + \sum_{j=1}^{M}(\sum_{i=1}^{M}) \frac{\mid c_{ij} \mid}{max_k \mid c_{kj} \mid -1} \tag{10}$$

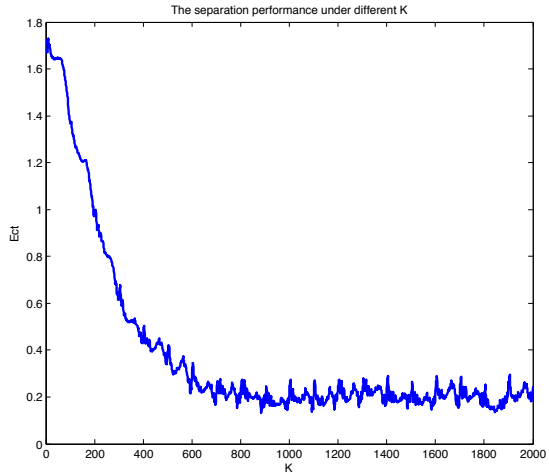

Fig. 6. Convergence Performance of the MOA algorithm.

From Fig.6, we can see that the algorithm has a good convergence performance, and it has a satisfied convergence speed.

C. Choosing the Parameters in MOA-algorithm

The MOA algorithm relys on a re-weighting procedure that penalizes certain entries of the estimated sources. The weights are function of the $\| \bullet \|_p$ norm of the columns of A. They somehow measure the activity of each sample across the sources. Intuitively, choosing a low value for p seems quite natural since it yields more contrast between sparse and non-sparse columns of A. This argument would make perfect sense if the true sources were known. A trade-off has to be made between the two following options [21]:

i) Large values for p might lead to an under-penalization of less discriminant entries.

ii) Small values for p provides a larger penalization of non-sparse entries of A, which is desirable to efficiently separate s.p.c. sources.

However, at the beginning of the MOA algorithm, one has only access to imperfect, if not erroneous, estimates of A. In this case, small values of p might mis-penalize/mis-favor entries of A which can eventually hamper the separation process. Alleviating this dilemma is made by starting with a high value for p-typically and then decreasing it, at each iteration, towards some final value p_f. Several values for p_f have been tested; it turns out that choosing $p_f = 0.001$ leads to a good trade-off for all the experiments we carried out. Smaller values for p_f did not bring any noticeable improvement [22].

D. Discussion About the Impact of Noise

In this section, we discuss the impact of the re-weighting scheme on the performances of the MOA in the noisy condition. First, in the MOA algorithm, the weights λ_i are estimated from the estimated sources. These sources are obtained via Step 1 of the MOA algorithm. In the low noise limit, one interesting feature of the proposed re-weighting scheme is that it is inversely proportional to the amplitude of the columns of A. More precisely, this entails that large entries of A which are shared by several sources are more penalized than small entries with the same relative distribution across the sources. Strongly penalizing large and correlated entries is desirable since they are detrimental to the estimation of the mixed matrix and the sources [23]. In the noisy setting, the situation turns out to be rather different since small-amplitude samples are more likely perturbed by noise than large amplitude entries. On one hand, the proposed re-weighting procedure might be disastrous for the separation of the sources whether they are partially correlated or not. Indeed, since the weights are inversely proportional to the amplitude of the columns of the sources, the proposed procedure will tend to favor small entries which are more affected by the presence of noise. On the other hand, Step 1 of the MOA algorithm rejects entries with amplitudes smaller than some prescribed noise-dependent level. This should lower the impact of noise on the performances of the MOA algorithm [24].

In [18 25], the authors demonstrated that the MOA algorithm is robust to additive noise contamination. This is especially true whenever morphological diversity holds; in that case the most discriminant sources are the entries of the sources with the most significant amplitudes. It turns out these entries are also the least contaminated by additive noise. In the case of s.p.c. sources, the most discriminant sources are not necessarily the large-amplitude samples. A first consequence is that noise will be very likely to have a strong impact on the quality of the separation.

V. SIMULATION AND BLIND SOURCE SIGNAL SEPARATION RESULTS

In this section, we present computer simulations, in order to illustrate the performance of the proposed MOA-algorithm. In the simulation, the non-orthogonal frequency hopping signal in time-frequency domain will be separated from the mixed signals.

Each parameter is defined as follows: $fb = 2 * 10^5 Hz$ for sample rate, $Rb = 10^3 bps$ for transmission bit rate, $v = 500 hop/s$ for hopping speed, $f_0 = 2 * 10^3 Hz$ for modulation frequency, $m = 8$ for bit numbers, the original signal numbers as $MK = 3$, and the receiving antenna numbers as $RK = 2$.

The sent source signal's Time-Frequency images are shown in the Fig.7. We aim to separate each object signal from the received mixed signals.

After Gauss channel transitions, the received mixed signal Time-Frequency images are shown in Fig.8 (Received Composite Signal). Here, we consider two channels to fully simulate the realistic signal transmission, which are shown from top row to the bottom row in Fig.8, respectively.

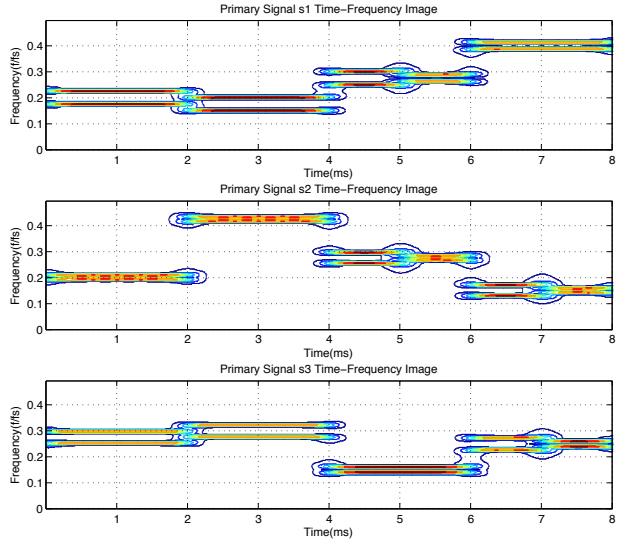

Fig. 7. The sent source signals waveforms. Three sent source signals are considered.

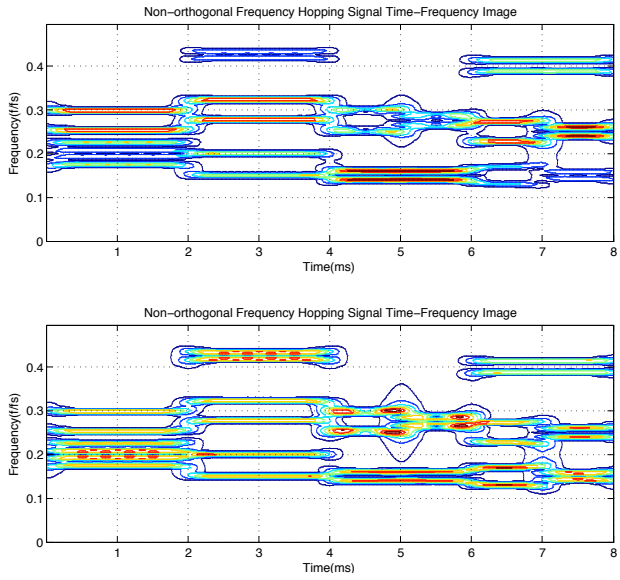

Fig. 8. The Received Mixed Signal Waves after Gaussian Channels. Two Gaussian Channels are considered.

A. The First Comparative Experiment of Effect

By using the proposed MOA-algorithm, the final blind source separation waveforms are shown in Fig.9, where three signals are displayed. It is seen that the obtained three object signals are very similar to the initial object signals in Fig.7.

We compare the signals between Fig.7 and Fig.9 by objective evaluation and further compare the separation performance with the classical searching and averaging method in frequency domain (SAMFD) [26], the Pearsons correlation coefficient value is used [27]. The results are shown in Fig.10, where

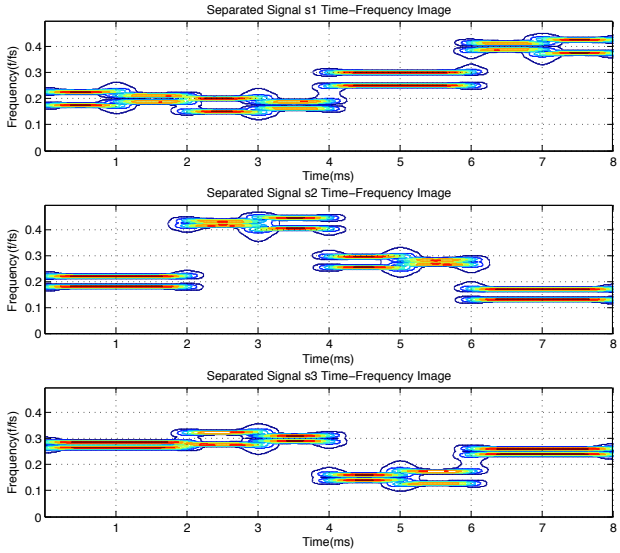

Fig. 9. Blind Source Separation Waveform Using the Proposed MOA-algorithm

Pearsons correlation coefficient is defined as:

$$r = \frac{\sum_{i=1}^{n}(x_i - \bar{x})(y_i - \bar{y})}{\sqrt{\sum_{i=1}^{n}(x_i - \bar{x})^2 \sum_{i=1}^{n}(y_i - \bar{y})^2}} \tag{11}$$

From Fig.10, we can see that blind sources signals can be efficiently separated by the MOA-algorithm, and it has a better performance than the classical SAMFD.

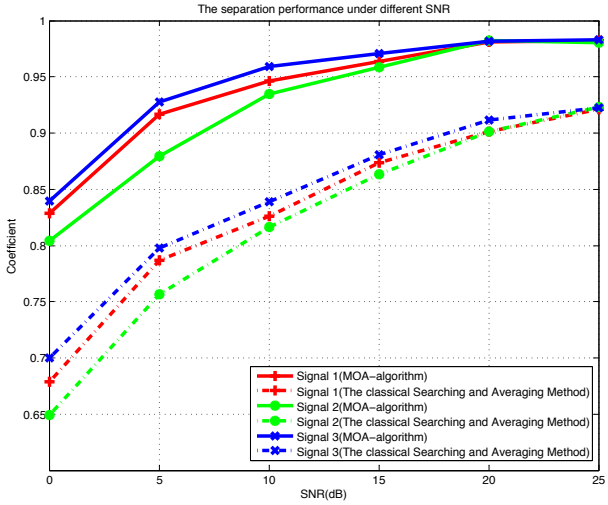

Fig. 10. Blind Source Separation Result, this article method has a better performance than classical Searching and Averaging Method

B. The Second Comparative Experiment of Effect

From the above section, we can know the MOA-algorithm has a satisfying separation effect. In the following section, we will analyse the separation effect by using the error performance analysis as another evaluation criterion. In the error performance analysis, we further compare the separation performance with the classical Based on the Ratio Matrix Clustering Algorithm [28], where the PI value is used [29]. The formula is defined as:

$$PI = E\{\frac{\| A \| - \| \widehat{A} \|}{\| A \|}\}, \tag{12}$$

here A is the mixed matrix, $\widehat{A}$ is the mixed estimation matrix. From Fig.11, we can see that blind sources signals can be

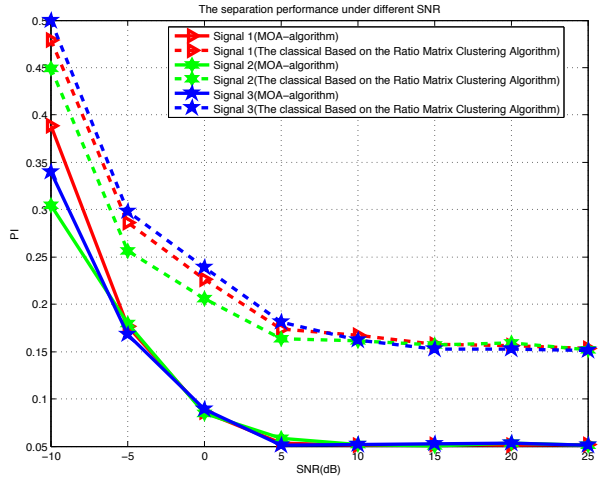

Fig. 11. Blind Source Separation Result, this article method has a better performance than classical classical Based on the Ratio Matrix Clustering Algorithm

efficiently separated by the MOA-algorithm, and it has a better performance than the classical Based on the Ratio Matrix Clustering Algorithm.

VI. CONCLUSION

In this paper, we propose non-orthogonal frequency hopping signal underdetermined blind source signal separation. Firstly, we introduce the relevant knowledge about blind source separation. Secondly, we design a novel MOA-algorithm to separate the mixed non-orthogonal FH signals. The experiment results demonstrate the effectiveness of the proposed method.

ACKNOWLEDGMENT

This work is fully supported by a grant from the national High Technology Research and development Program of China (863 Program) (No.2012AA01A502),and National Natural Science Foundation of China (No.61179006),and Science and Technology Support Program of Sichuan Province (No.2014GZX0004).

REFERENCES

[1] Ondrej Tichy and Vaclav Smidl, Bayesian Blind Separation and Deconvolution of Dynamic Image Sequences Using Sparsity Priors, IEEE Transactions on Medical Imaging, Vol.34, No.1, Jan.2015, pp.258-266.

[2] Matt Atcheson, Ingrid Jafari, Roberto Togneri, Sven Nordholm, on The Use of Contextual Time-Frequency Information for Full-Band Clustering-Based Convolutive Blind Source Separation, IEEE International Conference on Acoustic, Speech and Signal Processing (ICASSP), pp.2114-2118.
[3] Leonardo T. Duarte, Joao M.T.Romano, Senior Member, Christian Jutten, Karin Y. Chumbimuni-Torres, and Lauro T. Kubota, Application of Blind Source Separation Methods to Ion-Selective Electrode Arrays in Flow-Injection Analysis, IEEE Sensors Journal, Vol.14, No.7, July.2014, pp.2228-2229.
[4] Belouchrani A, Abed-Meraim K, Cardoso JF, etal., A blind source separation technique using second order statistics, IEEE Transactions on Signal Processing, Vol.45, No.2, 1997, pp.434-444.
[5] Zhi-Chao Sha, Zhi-Tao Huang, Yi-Yu Zhou, Feng-Hua Wang, Frequency-hopping signals sorting based on underdetermined blind source separation, IET Communications, 2013, Vol.7, Iss.14, pp.1456-1464.
[6] Jerome Bobin, Jeremy Rapin, Anthony Larue, and Jean-Luc Starck, Sparsity and Adaptivity for the Blind Separation of Partially Correlated Sources, IEEE Transactions on Signal Processing, Vol.63, No.5, March 1, 2015.
[7] Sun Long Wang, Wei Chen, Ning Hua Zhu, Jian Guo Liu, Wen Ting Wang, Jin Jin Gu, A Novel Optical Frequency-Hopping Scheme for Secure WDM Optical Communications, IEEE Photonics Journal. Frequency-Hop Scheme for WDM Communications, Vol.7, No.3, June 2015.
[8] Fangyuan Nan, SVD reconstruction algorithm and determination of signal number by frequency domain information, Antennas and Propagation Society International Symposium, vol.1, 1995,pp.428-430.
[9] Mohamed Anis Loghmari, Mohamed Saber Naceur, and Mohamed Rached Boussema, A New Sparse Source Separation-Based Classification Approach, IEEE Transactions on Geoscience and Remote Sensing, Vol.52, No.11, November 2014, pp.6924-6936.
[10] DIMITRI P. BERTSEKAS, On the Goldstein-Levitin-Polyak Gradient Projection Method, IEEE Transactions on Automatic Control, Vol.21, No.2, April 1976,pp.174-183.
[11] Arvind Ganesh, Zihan Zhou, Yi Ma, Separation of A Subspace-Sparse Signal: Algorithms And Conditions, IEEE International Conference on ICASSP 2009, pp.3141-3144.
[12] J.Bobin, J.L.Starck, M.J.Fadili, and Y.Moudden, Sparsity andmorphological diversity in blind source separation, IEEE Trans. Image Process., Vol.16, No.11, pp.2662-2674, 2007.
[13] J.Bobin, J.L.Starck, Y.Moudden, and M.J.Fadili, Blind source separation:The sparsity revolution, Adv. Imag. Electron Phys., Vol.152, pp. 221-306, 2008.
[14] P.L.Combettes and V.R.Wajs, Signal recovery by proximal forwardbackward splitting, SIAM J. Multiscale Model. Simulat., Vol.4, No.4, pp.1168-1200, 2005.
[15] Bernard Widrow, J.Mccool, A comparison of adaptive algorithms based on the methods of steepest descent and random search, IEEE Transactions on Antennas and Propagation, September 1976, pp.615-637
[16] A.Bruce, S.Sardy, and P.Tseng, Block coordinate relaxationmethods for nonparametric signal de-noising, in Proc. SPIE-The Int. Soc. for Opt. Eng., 1998, Vol.3391, pp.75-86.
[17] Paul Tseng, A coordinate gradient descent method for nonsmooth separable minimization, Mathematical Programming, March 2009, Volume 117, Issue 1, pp.387C423.
[18] Wotao Yin, Stanley Osher, Donald Goldfarb, and Jerome Darbon, Bregman Iterative Algorithms for ℓ_1-Minimization with Applications to Compressed Sensing, SIAM Journal on Imaging Sciences, Volume 1, Issue 1, pp.143C168.
[19] E.J.Candes, M.B.Wakin, and S.P.Boyd, Enhancing sparsity by reweighted l_1 minimization, Journal Fourier Anal. Appl., Vol.14, pp.877C905, 2007.
[20] Bin Li,Ruogu Li,, and Atilla Eryilmaz, On the Optimal Convergence Speed of Wireless Scheduling for Fair Resource Allocation, IEEE/ACM Transactions on Networking, Vol. 23, No. 2, April 2015, pp.631-643.
[21] Jerome Bobin, Jeremy Rapin, Anthony Larue, and Jean-Luc Starck, Sparsity and Adaptivity for the Blind Separation of Partially Correlated Sources, IEEE Transactions on Signal Processing, Vol.63, No.5, March 1, 2015, pp.1199-1213.
[22] John Canny, Computational Approach to Edge Detection, IEEE Transactions on Pattern Analysis and Machine Intelligence, Vol. PAMI-8, No. 6, November 1986, pp.679-698.
[23] Emmanuel J. Candes, Justin Romberg, and Terence Tao, Robust Uncertainty Principles: Exact Signal Reconstruction From Highly Incomplete Frequency Information, IEEE Transactions on Information Theory, Vol. 52, No. 2, February 2006, pp.489-509.
[24] Irina F. Gorodnitsky, and Bhaskar D. Rao, Sparse Signal Reconstruction from Limited Data Using FOCUSS: A Re-weighted Minimum Norm Algorithm, IEEE Transactions on Signal Processing, Vol.45, No.3, March 1997, pp.600-616.
[25] J. Bobin, J. L. Starck, M. J. Fadili, and Y.Moudden,Sparsity and Morphological Diversity In Blind Source Separation, IEEE Trans. Image Process. Vol.16, No. 11, 2007, pp.2662C2674.
[26] Olivier Meste, Herve Rix, Pere Caminal, and Nitish V. Thakor, Ventricular Late Potentials Characterization in Time Frequency Domain by Means of a Wavelet Transform, IEEE Transactions on Biomedical Engineering, Vol. 41, No. 7, July 1994, pp.625-634.
[27] S. M. Hassan Hosseini, Mehdi Vakilian, and Gevork B. Gharehpetian, Comparison of Transformer Detailed Models for Fast and Very Fast Transient Studies, IEEE Transactions on Power Delivery, Vol. 23, No. 2, April 2008, pp.733-741.
[28] Tao Xiang, and Shaogang Gong, Video Behavior Profiling for Anomaly Detection, IEEE Transactions on Pattern Analysis and Machine Intelligence, Vol. 30, No. 5, May 2008, pp.893-908.
[29] Nikolaos P. Papanikolopoulos, Pradeep K. Khosla, and Takeo Kanade, Visual Tracking of a Moving Target by a Camera Mounted on a Robot: A Combination of Control and Vision, IEEE Transactions on Robotics and Automation. Vol.9, No.1, February 1993, pp.14-35.

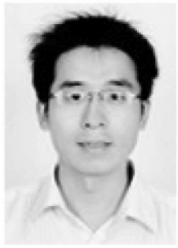

Chengjie Li received the B.Sc. degree in Shandong normal University, Qufu(Confuciuss hometown), China, 2004, the M.Sc. degree in applied mathematics in Xihua University, Chengdu, China, 2010. Now Chengjie Li is studying for Ph.D. degree in Communication and Information System in University of Electronic Science and Technology of China (UESTC), Chengdu, China, 2013.

Lidong Zhu received the B.S and M.S from Sichuan University, Chengdu, China, in 1990 and 1999, respectively, and the Ph.D. degree in Communication and Information Systems form Electronic Science and Technology of China, Chengdu, China, in 2003. From July, 2009 to June 2010, he was a visiting scholar with Department of electronic engineering of The University of Hong Kong. His research interests include satellite communications, blind source separation, and communication countermeasure.

Zhen Zhang received the B.Sc . degree in Sichuan University, 2005. Received the M.Sc degree in Xihua University, 2010. Now Zhen Zhang is working in NCS. Her research interests include channel code, signal processing, and intelligent information processing.

Estimation of the Clutter Correlation Coefficient in Radar Systems

Dmitrii I. Popov, Sergey M. Smolskiy, *Member, IEEE*[1]

***Abstract*. Estimation of passive interference (so-called, a clutter), which is caused by the point objects, is considered for radar systems. The initial sequence of sampled correlated readings of the point (in distance) target is used as an initial one causing by the antenna beam scanning in a surveillance radar. Basing on the statistical description of this sequence, the likelihood function is introduced and its properties are discussed. An estimation algorithm of the clutter correlation coefficient is synthesized according to the sample of initial correlated readings using the maximal likelihood approach. A structural scheme is given for the correlation coefficient measuring system. The clutter correlation coefficient estimations obtained are asymptotically effective. On the base of the Cramer-Rao equation, the asymptotic formula for a variance of the correlation coefficient is derived, which determines a dependence of estimation accuracy on the value of the correlation coefficient and a number of averaged readings. The formula derived allows provision of necessary estimation accuracy by means of appropriate choice of the averaged reading number. Statistical modeling of the estimation algorithm is described and performed. Modeling results are given, which characterize a dependence of estimation accuracy of the clutter correlation coefficient upon the averaged readings number. A comparison of theoretical and empirical results for estimation accuracy analysis is performed. Statistical modeling results confirm the asymptotical character of the estimation accuracy of the clutter correlation coefficient.**

Keywords: correlation coefficient, clutter, estimation algorithm, estimation accuracy, statistical modeling

I. INTRODUCTION

Since the time of the Second World War and till the present days, passive interference is the effective measure of antiradar camouflage [1, 2]. Since then, one of the relevant and difficult problems of detection of moving target signals on the passive interference background remains invariably during design and operation of radar systems. Passive interference in the form of spurious reflections from the fixed or slowly moved objects (so-called, clutter): local objects, land or sea surface, hydrometeors (clouds, rain, hail, snow) and metallized reflectors dropped for target masking, essentially disturb the normal operation of various radar systems [2]. The clutter intensity may essentially exceed the level of the receiver inherent noise, which leads to overloading of the reception channel (so called, radar "blinding") and hence to useful signal missing. Nevertheless, even for overloading absence, the useful signal may be lost or not detected at all on the background of intensive spurious reflections.

Imperfection of analogous devices (ultrasonic delay lines, barrier-grid storage tubes) hindered a progress in development of protection means against the passive interference [3]. Application of digital signal processing allowed implementation of the sub-optimal processor on the base of a digital filter for clutter suppression with further discrete Fourier transform of samples [4-6]. Utilization of digital approaches leads to creation of rejection filters with adaptation to the clutter Doppler phase [7, 8]. Development of digital methods and devices for digital signal processing goes on at present to discuss in the modern scientific-technological literature [9-11].

Up-to date stage of this area development, *a priori* ambiguity of the spectral-correlation clutter characteristics as well as their heterogeneity and non-stationarity in the observation zone essentially hamper implementation of effective detection of moving objects on the clutter background, which stimulate innovations in radar systems and processing methods for radar signals. Overcoming of *a priori* ambiguity of clutter parameters is based on processing algorithm optimization depending on clutter parameters and further replacement of unknown parameters by their reasonable estimations [12] according to the adaptive Bayesian approach. These estimations can be obtained according to learning samples in the form of readings in the adjacent resolution bins in range od the Doppler frequency, which leads to adaptive algorithm and processing systems creation.

The adaptive detection of signals from movable targets on the clutter background, which is created by unwanted reflections from the lengthy objects, is described in [13]. The point (in range) interference corresponding (in range) to signals reflected from the point (in range) targets requires the special attention, which, in some cases, cannot be distinguished from the moving targets. Publications [14-17] are devoted to problems of surveillance radar system protection against this type of interference. That is why, it is interesting to have the estimation algorithms, which take into account the point character of the clutter.

Manuscript submitted on September 9, 2016.

[1] Dmitrii I. Popov is with Ryazan State Radio Engineering University, Russia (e-mail: adop@mail.ru).
Sergey M. Smolskiy is with Moscow Power Engineering Institute (National Research University), Russia (e-mail: SmolskiySM@mail.ru).

Estimates of maximal likelihood have found the most distribution since they are un-biased (or asymptotically unbiased) and asymptotically effective. In problems of signal detection, the clutter correlation coefficients [13] are, as a rule, the estimating parameters. At that, the detection effectiveness depends on estimation accuracy. In this connection, the estimation algorithm's choice and the point clutter accuracy analysis are a relevant issue. Algorithms and estimation accuracy of the clutter correlation coefficient are considered below according to the sample of the correlated readings of the point clutter.

II. SYNTHESIS OF THE ESTIMATION ALGORITHM

Now we consider a solution of stated problem in the coherent-pulse surveillance radar system, which performs the discrete of continuous space observation. Let it be a sequence of n sampled correlated readings of the point (in range) clutter at the output of linear portion of a receiver. This sequence is caused by the antenna beam scanning in the surveillance radar and presented in the following form: $\{u_j\}^{(n)} = \{u_1, u_2, \dots, u_n\}$. The estimation algorithm and the statistical estimation error result from statistical description of the given sample of readings caused by the fluctuation character of the spurious reflections.

Multiply reflection character leads to their Gaussian statistical description, being in this case adequate, the most reliable and experimentally confirmed [2]. The variation of reflection points, a height and range of the clutter source are taken into account in estimation results of required parameters, which is exactly the goal of the empirical approach to solution of this problem. Utilization of another model (not Gaussian) requires its reasonable choice experimentally substantiated and a presence of opportunities to describe the selective clutter properties, in particular, spectral properties. Use of the Markovian theory [18] for description of non-Gaussian signals turns out to be unpractical and unproductive. The Markovian model does not take into account the selective properties of signals and interference being as a matter of fact of non-coherent description and does not lead to practical circuits and devices, which allow extraction of moving target signals on the background of interference with surpassed power [18].

At Gaussian fluctuation character, the corresponding statistical description is given by a likelihood function (LF)

$$P(\{u_j\}^{(n)} / \rho) = (2\pi)^{-\frac{n}{2}} \det^{-\frac{1}{2}}[r_{jk}] \times \times \exp\left(-\frac{1}{2} \sum_{j,k=1}^{n} w_{jk} u_j u_k \right), \quad (1)$$

where $r_{jk} = \sigma^2 \rho_{jk}$ are elements of a clutter correlation matrix; σ^2 is the clutter variance; ρ_{jk} are correlation coefficients of the clutter readings; w_{jk} are elements of the reverse correlation matrix $[w_{jk}] = [r_{jk}]^{-1}$ of the clutter.

For interference in the form of the simply connected Markovian sequence, the correlation function has exponential character. Then, elements $\rho_{jk} = \rho^{|j-k|}$ and $r_{jk} = \sigma^2 \rho^{|j-k|}$. In this case

$$\det[r_{jk}] = \sigma^{2n} (1-\rho^2)^{n-1}, \quad (2)$$

and elements of the reverse correlation matrix are

$$\left.\begin{aligned} &w_{11} = w_{nn} = 1/\sigma^2(1-\rho^2), \\ &w_{jj} = (1+\rho^2)/\sigma^2(1-\rho^2) \quad (1 < j < n), \\ &w_{j-1,\,j} = w_{j,\,j-1} = -\rho/\sigma^2(1-\rho^2) \quad (1 < j \le n). \end{aligned}\right\} \quad (3)$$

Other elements w_{jk} equal to zero.

To solve this problem, we use the maximal likelihood method, which universality and relative simplicity combines with great achievements of estimations obtained, which are always (under condition of likelihood equation solution uniqueness) true, asymptotically normal and asymptotically effective [12, 19]. The estimation algorithm for the correlation coefficient ρ we find from the likelihood equation

$$\partial \ln P(\{u_j\}^{(n)} / \rho) / \partial\rho \Big|_{\rho=\hat{\rho}} = 0.$$

For this, at first, we take the logarithm from LF (1):

$$\ln P(\cdot) = -\frac{n}{2} \ln(2\pi) - \frac{1}{2} \ln\det[r_{jk}] - \frac{1}{2} \sum_{j,k=1}^{n} w_{jk} u_j u_k .$$

Taking into consideration the expression (2) and elements of the revere matrix (3), neglecting by edge effects of the main diagonal, we find

$$\ln P(\cdot) = -\frac{n}{2} \ln(2\pi) - \frac{1}{2}[\ln\sigma^{2n} + (n-1)\ln(1-\rho^2)] - -\frac{1+\rho^2}{2\sigma^2(1-\rho^2)} \sum_{j=2}^{n} u_j^2 + \frac{\rho}{\sigma^2(1-\rho^2)} \sum_{j=2}^{n} u_{j-1} u_j . \quad (4)$$

As a result of differentiation of (4), we have

$$\frac{\partial \ln P(\cdot)}{\partial\rho} = \frac{(n-1)\rho}{1-\rho^2} - \frac{2\rho}{\sigma^2(1-\rho^2)^2} \sum_{j=2}^{n} u_j^2 + + \frac{2\rho^2}{\sigma^2(1-\rho^2)^2} \sum_{j=2}^{n} u_{j-1} u_j + \frac{1}{\sigma^2(1-\rho^2)} \sum_{j=2}^{n} u_{j-1} u_j . \quad (5)$$

Now the likelihood equation has a form

$$\frac{(n-1)\rho}{1-\rho^2} - \frac{2\rho}{\sigma^2(1-\rho^2)^2} \sum_{j=2}^{n} u_j^2 + + \frac{1+\rho^2}{\sigma^2(1-\rho^2)^2} \sum_{j=2}^{n} u_{j-1} u_j \Bigg|_{\rho=\hat{\rho}} = 0 .$$

After algebraic transformations, we obtain for the likelihood equation

$$(n-1)(1-\rho^2) - \frac{2}{\sigma^2} \sum_{j=2}^{n} u_j^2 + + \frac{1+\rho^2}{\sigma^2\rho} \sum_{j=2}^{n} u_{j-1} u_j \Bigg|_{\rho=\hat{\rho}} = 0 .$$

For the greatly-correlated clutter ($\rho \to 1$), the likelihood

equation takes a form

$$-\sum_{j=2}^{n} u_j^2 + \frac{1}{\rho}\sum_{j=2}^{n} u_{j-1}u_j\Bigg|_{\rho=\hat{\rho}} = 0,$$

from which we find the required estimation algorithm:

$$\hat{\rho} = \sum_{j=2}^{n} u_{j-1}u_j \Bigg/ \sum_{j=2}^{n} u_j^2 . \qquad (6)$$

This algorithm results from the statistical synthesis procedure, in essence, is optimal and allows the simple physical interpretation. Accumulation presented in the algorithm allows smoothing of obtained sample fluctuations, thereby increasing the estimation accuracy. The algorithm (6) can be expanded to a case of the clutter with arbitrary correlation properties.

A structural scheme of the correlation coefficient measuring system is presented in Fig.1, which realizes the algorithm (6), where SD is the storage device, × is a multiplier unit, Acc is an accumulator, D is a divider unit.

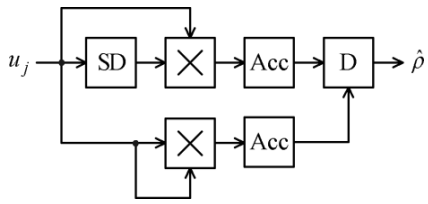

Fig. 1. A structural scheme of the correlation coefficient measuring system

III. ANALYSIS ON ESTIMATION ACCURACY

For future utilization of the correlation coefficient estimation $\hat{\rho}$, it is necessary to determine of its estimation accuracy. Taking into consideration that the obtained estimation $\hat{\rho}$ is asymptotically normal and asymptotically effective, we shall characterize the estimation accuracy by a variance of the correlation coefficient estimation $\hat{\rho}$, which is defined by the Cramer-Rao equation [19]:

$$\sigma_{\hat{\rho}}^2 = -\left[\overline{\partial^2 \ln P(\{u_j\}^{(n)} / \rho) / \partial\rho^2}\right]^{-1}. \qquad (7)$$

To make the appropriate calculations in (7), we find the second derivative of the likelihood function (1), by differentiation of (5):

$$\frac{\partial^2 \ln P(\cdot)}{\partial\rho^2} = \frac{(n-1)(1+\rho^2)}{(1-\rho^2)^2} + \frac{4\rho}{\sigma^2(1-\rho^2)^2}\sum_{j=2}^{n} u_{j-1}u_j - \frac{2(1+3\rho^2)}{\sigma^2(1-\rho^2)^3}\left(\sum_{j=2}^{n} u^2 - \rho\sum_{j=2}^{n} u_{j-1}u_j\right).$$

As a result of statistical averaging, taking into account that $\overline{u_{j-1}u_j} = \sigma^2\rho$, and $\overline{u_j^2} = \sigma^2$, we obtain

$$\overline{\frac{\partial^2 \ln P(\cdot)}{\partial\rho^2}} = \frac{(n-1)(1+\rho^2)}{(1-\rho^2)^2} + \frac{4(n-1)\rho^2}{(1-\rho^2)^2} - \frac{2(n-1)(1+3\rho^2)}{(1-\rho^2)^2} = -\frac{(n-1)(1+\rho^2)}{(1-\rho^2)^2}.$$

According to (7), we have finally:

$$\sigma_{\hat{\rho}}^2 = \frac{(1-\rho^2)^2}{(n-1)(1+\rho^2)}. \qquad (8)$$

As we see, the estimation accuracy depends on the correlation coefficient ρ and a number of averaged readings n. Evidently that the necessary accuracy of estimation can be provided by appropriate choice of the number of averaging readings n.

Expression (8) characterizes the potential accuracy of the measurement indicating the lower boundary of the variance $\sigma_{\hat{\rho}}^2$. Nevertheless, results of imitation statistical modeling of analyzed algorithms and signal processing devices are recognized by radar engineers as the most reliable and adequately represented the features of the actual devices.

IV. MODELING OF THE ESTIMATION ALGORITHM

Statistical modeling of the estimation algorithm includes formation of the model of an initial sequence of the clutter readings, calculation of the correlation coefficient estimation in accordance with the algorithm (6), and statistical determination of the estimate variance. Modeling is convenient to perform in the universal mathematical software package MathCAD, which is widely accepted as the best system for scientific-technological computations. The MathCAD package has powerful embedded means for implementation of numerical methods for calculations and mathematical modeling in combination with possibility to perform many operations of the symbolic mathematics.

Modeling of the initial clutter readings for the normal (Gaussian) distribution law and given correlation properties reduces to sequence formation of n sampled correlated readings.

To define a sequence of random numbers distributed by the normal law, we use the embedded element of random numbers, which is called in the MathCAD system by the function $\mathrm{rnorm}(m, \mu, \sigma)$, whose appropriate parameters are: m is a number of called elements, μ is mathematical expectation, σ is the rms deviation.

Formation of the initial sequence of correlated readings is done by means of linear transformation of random numbers, which are generated by the embedded element in the MathCAD system. In the case of the exponential correlation function $\rho_{jk} = \rho^{|j-k|}$, this linear transformation has a view:

$$u_j = \rho u_{j-1} + \sqrt{1-\rho^2}\,\mathrm{rnorm}(1,\ 0,\ 1), \quad j = \overline{1,\ n},$$

where $u_0 = \mathrm{rnorm}(1,\ 0,\ 1)$.

On the base of formed readings u_j, according to the algorithm (6), the correlation coefficient estimation $\hat{\rho}$ can be obtained.

By the method of statistical testing (the Monte-Carlo method) consisting of multiple repeat of the estimation algorithm (6) to estimate the correlation coefficient $\hat{\rho}$ we obtain the sample $\{\hat{\rho}_i\}$, $i = \overline{1, N}$, where N is a number of experiment repetitions.

The variance of correlation coefficient estimation is obtained from the following expression:

$$\sigma^2_{\hat{\rho}} = \frac{1}{N-1}\sum_{i=1}^{N}(\hat{\rho}_i - \mu_{\hat{\rho}})^2 \cong \frac{1}{N}\sum_{i=1}^{N}\hat{\rho}_i^2 - \mu^2_{\hat{\rho}},$$

where $\mu_{\hat{\rho}} = \frac{1}{N}\sum_{i=1}^{N}\hat{\rho}_i$ is the mathematical expectation or the mean value of the correlation coefficient estimation.

Figure 2 shows curves characterizing the dependence of the rms value of $\sigma_{\hat{\rho}}$ upon the readings number n at $\rho = 0.99$ and $N = 1000$. The solid curve corresponds to computations on the formula (8), and the dotted curve corresponds to empirical results obtained by means of statistical modeling on a computer.

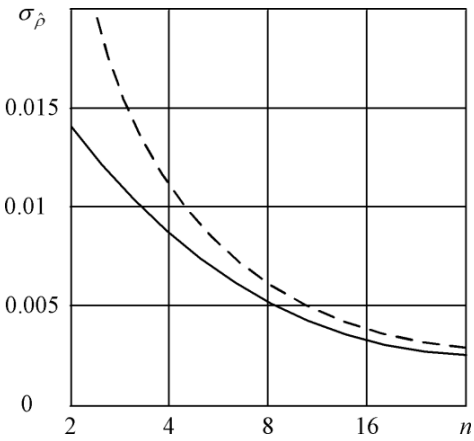

Fig. 2. Dependence of the rms value of $\sigma_{\hat{\rho}}$ upon the reading number n

Results obtained according to formula (8) have the asymptotical character approaching to the true measurement accuracy as n increase. Statistical modeling results confirm this circumstance. At $n = 8$ the modeling results differ from the calculation results basing on the formula (8) not more than by 20%. At $n > 8$ these differences are reduced accordingly, which confirms the asymptotical character

V. FUTURE INVESTIGATIONS

Results obtained in this paper are going to be used for optimization and analysis of the non-recursive rejection filterз.

In conformity with tasks of moving object selection on the background of lengthy passive interference, we are going to synthesize estimation algorithms for clutter correlation parameters: correlation coefficients and the Doppler phase shift, taking into account the interference structure. Moreover, we are going to analyze estimation accuracy depending on the clutter parameters and the volume of learning sample.

For rejection filters on non-recursive type, we hope to develop criteria and adaptation algorithms to unknown spectral-correlation characteristics of the clutter. On the base of approximating models of the clutter, we think to obtain stable (from computing point of view) algorithms of adaptive rejection of this clutter. We hope to develop structural schemes of adaptive rejection filters of sliding and grouped processing.

We are going to perform effectiveness analysis of non-recursive rejection filters versus the filter order, signal and clutter parameters, the volume of learning sample. We plan to solve problems of optimization under conditions of *a priori* ambiguity of signal detection systems on the background of the clutter, which perform the coherent rejection with further coherent or non-coherent accumulation of rejection remainders.

We hope to solve problems of parametric and structural optimization of detection systems for multi-frequency and non-equidistant signals on the clutter background. .

VI. CONCLUSION

The synthesized maximally-likelihood estimation algorithm (6) and the corresponding measuring device allow asymptotically effective estimations of the clutter correlation coefficient. The estimation accuracy, which characterize by formula (8) obtained for the clutter correlation coefficient, has the asymptotical character, which is confirmed by results of statistical modeling provided.

REFERENCES

1. Stepanov, Yu.G. Anti-Radar Camouflage (in Russian). – Moscow: Sovetskoe Radio, 1968. – 144 p.
2. Radar Handbook / Ed. by M. I. Skolnik. – 3rd ed. – McGraw–Hill, 2008. – 1352 p.
3. Vishin, G.M. Moving Target Selection (in Russisn)/ – Moscow: Voenizdat, 1966. – 276 p.
4. Rabiner, L. Theory and Application of Digital Signal Processing (in Russian)/ Rabimner L., Gold B. – Moscow.: MIR Publisher, 1978. – 848 p.
5. Popov, D.I. Optimization of radar systems of multichannel filtering (in Russian)// Izvestia VUZov-Radio Electronics. – 2000. – Vol. 43. – № 4. – P. 65-72.
6. Popov, D.I. Optimization of systems for coherent signal processing (in Russian)// Radiopromyshlennost. – 2016. – № 3. – P. 6-10.

7. Popov, D.I. Optimization of rejection filters with patial adaptation (in Russian) // Izvestia VUZov-Radio Electronics – 1998. – Vol. 41. – № 3. – P. 49-55.
8. Kuzmin, S.Z. Digital radar technology. Introduction to theory. – Kiev: KViC Publisher , 2000. – 428 p.
9. Skolnik, M.I., Introduction to Radar System, 3rd ed., New York: McGraw-Hill, 2001. – 862 p.
10. Barton, D.K. Radar System Analysis and Modeling, Norwood, MA: Artech House, 2005. – 534 p.
11. Richards, M.A.; Scheer, J.A.; Holm, W.A. (Eds.), *Principles of Modern Radar: Basic Principles*, SciTech Publishing, IET, Edison, New York, 2010 – 924 p.
12. Repin, V.G., Tartakovskiy G.P. Statistical synthesis for a priori ambiguity and adaptation on information systems (in Russian) / – Moscow.: Sovetskoe Rasdio. 1977. – 432 p.
13. Popov, D.I. Adaptive processing of signals against the background of passive interferences. *Radioelectron. Commun. Syst*., 2000, Vol. 43, No. 1, p. 50.
14. Lozovskiy I.F. Surveillance Radar Protection from the Point Interference – Novosibirsk: «Novosibirsk State Technical University Publisher», 2014. – 242 p.
15. Lozovskiy I.F. Growth of Effectiveness of Surveillance Radar Protection against point passive interference- Vestnik Vosdushno-Kosmicheskoi Oborony – 2014. – № 4 (4). – P. 45-49.
16. Lozovskiy I.F. Increase of Protectability of Surveillance radar against the point interference impact – Vestnik of Almaz-Antei Concern (in Russian)//, 2015. № 1 (13). P. 9-17.
17. Lozovskiy I.F. Construction and effectiveness of adaptive signal processing under conditions of combined interference impact // Uspekhi sovremennoi Radio Elektroniki (in Russian). – 2016. – № 1. – P. 52-58.
18. Sosulin Yu. G. Detection theory and estimation of stochastic signals (in Russian). – Moscow.: Sovetskoe Radio, 1978. – 320 p.
19. Cramer, H. *Mathematical Methods of Statistics*. *Princeton*: Princeton University Press, 1999. 648 p.

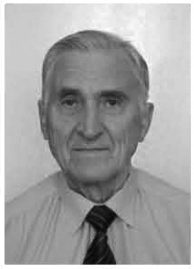

Dmitrii I. POPOV, born in 1939, in Ryazan, Ph.D. in Engineering, Dr. Sc. in Engineering, full professor of Radio Engineering Systems Department in Ryazan State Radio Engineering University (RSREU). Graduated from RSREU in 1961 on specialty "Designing and manufacture of radio equipment". Ph.D. from 1967, Dr.Sc. from 1990.
PhD thesis in specialty "Radar and Radio Navigation Technologies" on theme "Research of detection systems effectiveness for fluctuating signals on the clutter background". Dr.Sc. thesis in specialty "Radar and Radio Navigation Technologies" on theme "Synthesis and analysis of adaptive systems for moving target selection". The active member of International Academy of Informatization.
Author of about 320 scientific publication and patents. Field of research: theory and technique of radar signals processing against noises.

Sergey M. SMOLSKIY, born in 1946, Ph.D. in Engineering, Dr.Sc. in Engineering, full professor of Department of Radio Signals Formation and Processing of the National Research University "MPEI". After graduation of Ph.D. course and defense of Ph.D. thesis in 1974 he worked in Department of Radio Transmitting Devices of MPEI, where was engaged in theoretical and practical problems of development of transmitting cascades of short-range radar. In 1993 defended the Doctor of Science thesis and now he works as a professor of Radio Signals Formation and Processing Dept. Academic experience - over forty years. The list of scientific works and inventions contains over three hundreds of scientific articles, 15 books, three USSR copyright certificates on invention, more than 100 technological reports on various conferences, including international. The active member of International Academy of Informatization, International Academy of Electrotechnical Sciences, International Academy of Sciences of Higher Educational Institutions. The active member of IEEE. Honorary doctor of several foreign universities. The scientific work for the latter fifteen years is connected with conversion directions of short-range radar systems, radio measuring systems for fuel and energy complex, radio monitoring system etc.

Round-Robin Bloom Filters Based Load Balancing of Packet Flows

Örs Szabó and Csaba Simon

Abstract —**SDN gives the possibility to design new solutions for flow based load balancers, needed by the handling of quickly growing Internet data, and end user demands. A key element of this can be the Bloom filters and its probabilistic techniques to reduce information processing and networking costs. We selected a Bloom filter variant optimized for low footprint and designed and implemented a flow based load balancer solution. We identified an issue of such load balancers during their initialization phase in case of plug and play deployments. We propose a solution to alleviate this problem and evaluated its performance.**

Keywords- Bloom Filter; Load Balancing; packet flow

I. INTRODUCTION

Internet data traffic is quickly growing, as more and more people are getting easy access to different kinds of services, such as file sharing, video streaming, video-on-demand (VoD), IPTV, Voice-over-IP (VoIP), etc. Thus the data that needs to be transported from and to different nodes through a meshed network is increasing. This may cause capacity and performance issues on the serving nodes, which leads to the need of scaling. A commonly used technique is to group the serving nodes into a cluster, but still offer the service over a single access point (e.g., well known address). By doing so, the clients will still reach the service the same way as before. For this to work, a solution was needed to cleverly distribute the demand among the server cluster members. This functionality is provided by the load balancer: it tries to share the load within the cluster [1]. The packets transported over the Internet can be viewed as part of a session defined by the endpoints (e.g., source and destination addresses, port numbers).

The load balancer should be able to identify the different sessions (or flows) and should direct the packets belonging to it to the same server within the cluster. When the load balancer deals with flows, it has a dual task: it should both balance the load among the served output ports (assuming that each port leads to a different server) and to evenly distribute the amount of traffic among these ports. The problem is that the carried traffic volume might differ from flow to flow, thus it is not enough to focus on the per-flow traffic distribution. It is neither acceptable to focus solely on the equal traffic load distribution, because then different packets from the same flow would be sent out on different ports, potentially to different servers.

Most of the theoretical models that address the load balancing problem try to provide a solution optimizing the resource usage of the control process and/or focus on the long term stability of traffic load distribution. (see the rest of this Section). Nevertheless, the proper operation of a load balancing mechanism is vulnerable to the initialization of the mechanism itself, as we learned it during the implementation and testing of a stateful load balancing proposal (called Round Robin Bloom Filter) optimized in terms of resource usage. In what follows we introduce the reader into our motivation to work with and the environment in which we implemented the particular load balancing solution. Later on in the paper (see Section IV.C) we show how does this initialization problem (named *startup transient*) manifest in a backbone network by conducting dedicated experiments with our implementation. Further on we propose a solution to alleviate this problem and discuss its applicability using further experiments. Thus the main contribution of our paper is to show how the startup transient issue was handled, as it has a crucial role in sustaining the balance between the dual role of load distribution and flow integrity preservation of a stateful load balancer.

When we searched for potential environments to design and deploy a load balancer, we quickly converged to a decision on selecting Software-Defined Networking (SDN), as it is widely recognized as an enabler of dynamic network behavior to adapt to changes in demand [2]. The use of SDN to respond to increasing load is a natural choice and has already been investigated by the networking community. Load balancing in SDN can be achieved in different ways, one of which is to use Finite State Machine (FSM) models with defined network policies described in [3]. Nevertheless, the memory footprint and the required reaction speed for such solution when we have to control a backbone link of the networks calls for the use of new mechanisms. We oriented ourselves towards probabilistic techniques, as many of the network solutions today utilize them to reduce information processing and networking costs. Having millions of data elements in any network it became increasingly important to develop efficient solutions for storing, updating, and querying them. One great idea introduced by Bloom filters (BF) is that by allowing the representation of the set of elements to lose some information, the storage requirements can be significantly reduced [4]. The BF is a space-efficient probabilistic data structure that supports

The authors are with the HSN Lab, Department of Telecommunication and Media Informatics, Budapest University of Technology and Economics, Budapest, Hungary (email: simon@tmit.bme.hu)

set membership queries. This data structure provides a probabilistic way to represent a set that can never have false negatives (saying that an inserted element is not in the set) but can have false positive returns (saying that an element is part of the set when in fact it is not).

Networking applications of different BFs emerged back in the late 90s. Broder and Mitzenmacher published a survey [5] on network applications of BFs in 2004. A very recent survey [2] by Tarkoma et al. from 2012 reviews over 20 BF variants and their applications for caching, peer-to-peer systems, routing and forwarding, and measurement data summarization. For our work, the interesting application field of Bloom filters is the flow based load balancing.

Regardless of the wide range of different BF flavors, we found that apart of the proposal of Szabo in [6] no suitable BF adaptation for efficiently applying actions consistently to an event stream, based on past decisions assigned to events within a time window. This solution retains the control states assigned to subset of events according to their arrival time slot up to a time window. The Round-robin Bloom filters (RRBF) proposed there would suit well the server farm load sharing or the path load balancing scenarios. An alternative proposal was the Time-Decaying Bloom filter (DBF) [7], which uses bounded counters in each filter bit position. It increments by 1 at the hash positions of the tested/inserted item and decreased, and decreases it periodically each counter. Two proposals were made to add duplicate flow detection to Bloom Filters. Shen and Zhang in [8] proposed to use a DBF and a BF in pair together with a counting sliding window, while Changling et al. in [9] used a time-based sliding window together with a Round robin Buddy Bloom Filter structure. Nevertheless, both these proposals omit the possibility to distribute flows over multiple filters. A different approach from the above ones, using the adaptive highest random weight (HRW) method to account for the uneven flow size popularity, is described in [10].

Note that it is possible to extend the BF scheme of [6] to counting sliding windows. Counting filters provide a way to implement a delete operation on a Bloom filter without recreating the filter afresh. Counting filters were introduced by Fan [11], proposing to extend the filter positions from a single bit to an n-bit counter. These filter variants require more memory space than the basic Bloom filters, as it have to store the value of the counter.

In the following Section II we present the Round-Robin Bloom Filter (RRBF) analysis, summing up those parts of the RRBF proposal that are interesting for our work. We designed and implemented a flow based load balancer solution using RRBF supporting plug and play deployment, the details of design and implementation being presented in Section III. We ran a set of experiments in an emulated environment. In Section IV we discuss the startup transient issue occurring at the time when starting up or connecting the load balancer to the network and the evaluation of our solution to this issue. Finally Section V concludes our work.

II. ROUND-ROBIN BLOOM FILTER

A. Background

The accuracy of the Bloom filter depends on the filter size (m), the number of hash functions (k), and the number of elements included (n). The more elements are added to a Bloom filter, the higher the probability that the query operation reports false positives. A Bloom filter requires space O(n) and can answer membership queries in O(k) time. The below **TABLE 1** examines the behavior of the three key parameters when their values are either decreased or increased.

TABLE 1
BLOOM FILTER KEY PARAMETERS

Bloom Filter parameters	Increase
Number of hash functions (k)	More computation, lower false positive probability as $k \to k_{opt}$
Size of filter (m)	More space is needed, lower false positive probability
Number of elements in the set (n)	Higher false positive probability

Increasing or decreasing the number of hash functions towards k_{opt} we can lower the false positive probability but the computations for the insertions and lookups will increase. The cost is directly proportional to the number of hash functions. A larger filter will result in fewer false positives.

The calculation of false positive probabilities and the optimal number of hash functions for that is derived in [6]. It is shown that the false positive probability decreases as the size of the Bloom filter (m) increases, and it increases as more elements are added (n). In order to maintain a fixed false positive probability, the length of a Bloom filter must grow linearly with the number of elements inserted in the filter. The optimal Bloom filter size (m) for the expected number of elements (n) and false positive probability (p), is described in [6].

B. Round-Robin Bloom Filter

Once a member is added to a BF, it cannot be deleted – during the lifetime of a BF, after a certain operation time it starts to be inefficient, because lots of expired flows are still referenced in the BF. In order to improve the applicability of BFs, several mechanisms were proposed to allow deleting members from BFs, as presented in the previous section. One of the most efficient solutions is the Round-Robin Bloom Filter (RRBF).

The design of the RRBF is presented based on [6]. The operations over the RRBF are defined as follows:

- *Membership query*: we query for the existence of an event from the oldest to youngest filters and if a match is found then a corresponding action is executed without further queries.
- *New element insert*: if no match is found during the membership query, then the event is inserted into the youngest filter.

- *Window jump*: before entering into the next time slot, we reset the oldest filter and make a jump to select the next youngest and oldest filters.

In the following we explain in brief the operation of a RRBF, summing up the detailed description from [6]. Fig. 1 presents an example of the RRBF operation. In each time slot, only one filter (red) will be used to insert new elements, while the others (cyan) are queried in decreasing age order. After N time slots, the oldest filter is reset and the next oldest and youngest filter will be selected in a round-robin fashion. When the event $e(\tau)$ arrives in the 7th time slot, its hash is tested for containment in filters v_4; v_5; v_1; v_2 sequentially. If a match is found, the corresponding A_i action is executed and further querying is stopped. If no match is found, the event is inserted into filter v_3 (the latest filter marked with red) and the corresponding A_3 action is executed.

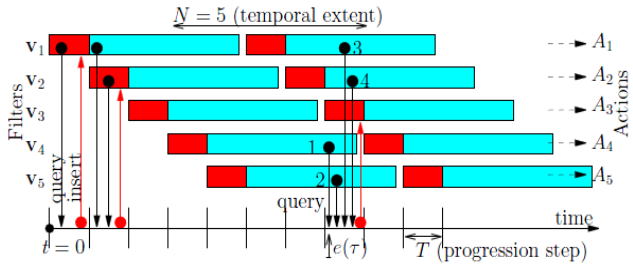

Fig. 1 Round-Robin Bloom Filter design (source: [6])

If we treat the incoming events as IP packets and their fingerprints being calculated from their IP headers, which we can call individual flows, then we can see that a consecutive number of packets of the same flow will have the same action executed, at least for *(N-1)*T* times, after which a reroute can happen. Assigning different output ports for the different actions means that we can create a load balancing solution among alternative paths.

III. FLOW BASED LOAD BALANCER: DESIGN & EXPERIMENTS

In the previous sections we introduced RRBF, as a candidate solution to support efficient load balancing for large number of flows – typically in the backbone links. In this section we present an implementation of this system. Since the packet based networks are very dynamic and diverse, the implementation should be flexible, easily configurable and customizable. During the traffic engineering process the controlled flows, the available paths and the associated ports may change in time, which results in the request to change the RRBF configuration and the port assignments.

SDN has been introduced in the last decade in computer networking to address this issue, separating the control and data planes from each other, and putting an open interface in-between [2]. The cornerstone of the SDN framework is the control protocol over this interface that commands the switches, called OpenFlow. Having freedom in the control plane it gives room for innovation and makes the implementation of such a complex control process practically feasible.

A. Design

We show the design of the load balancer prototype supporting plug and play deployment by eliminating the startup transient at system start time. The issues presented in Section I. were considered during implementation, and the prototype was built in a way that the RRBF solution could be verified with different traffic characteristics. The system consists of the following modules:

- *Emulated environment* – provided by Mininet [12].
- Emulated *OpenFlow controller* – used to configure the switch with the necessary ports, tables and actions. Each table will have a different role, e.g., to match IP packets, select Bloom filters or select output ports.
- Emulated *OpenFlow switch* [13] – implemented with internal RRBF system parameters, e.g. expected number of ingress flows, desired false positive probability, etc.

During the implementation of these modules we reused the open source Bloom filter code of Virkki [14] and the MurmurHash2 code of Appleby [15].

Fig. 2 shows the designed internal structure of the RRBF load balancer. There is only one flow table with one flow entry. The input port is passing all ingress packets to the flow entry. All packets are matched against the condition, eth_type=0x800, that is only IP packets will be processed further. The flow entry will pass the packets to the first group entry in the group table. Each bucket of the group entry contains a Bloom filter. Based on the Round-robin Bloom filter algorithm one bucket will be selected. Each bucket has the same action, passing the packets to the next group entry. The next group entry has a number of buckets, each associated with an output port. Based on the output port selection algorithm the packets will be sent out from one of the output ports.

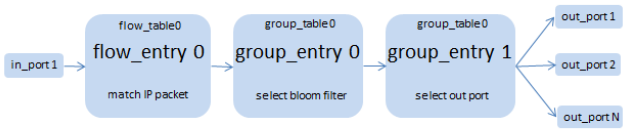

Fig. 2 Internal architecture of the RRBF based load balancer

B. Control mechanism

The following system parameters are implemented and can be controlled:

- Number of Bloom filters (B) – it's set by the controller via the OpenFlow protocol.
- Number of output ports (P) – it's set by the controller via the OpenFlow protocol.

- Packet type – it is set by the controller via the OpenFlow protocol.
- Period (*T*) – time period in seconds after which there is a shift in Bloom filters, and the next one will be the youngest accepting new flows.
- Epoch (*Ep*) – time period for the youngest Bloom filter until it becomes the youngest again, i.e. *(B-1)*T* seconds.
- False positive probability (*E*) – used to calculate the number of hash functions (*K*) for the Bloom filters.
- Number of elements (*N*) – number of expected flows per Bloom filter and it is used to calculate the size (*M*) of the Bloom filters.
- Transient packets (*Tr*) – used to set the number of packets to be used at the beginning for flow transient elimination.
- Redistribution threshold (*R*) – used to decide if new output port can be associated with a filter depending on the number of the ingress packets in the last period (*T*) compared to the number of ingress packets in the last epoch (*Ep*).

The first two parameters define the structure of the RRBF mechanism, whereas the *T* and *Ep* parameters define its dynamics. Once the number of BFs within the scheme is fixed, the memory footprint of the RRBF depends on the *E* and *N* parameters.

The effect of the *Tr* and *R* parameters determine the efficiency of the load balancing process. *Tr* affects the reaction of the mechanism at startup, as detailed in Section III.E. Note that according to the original proposal we should only select a new port for a BF if all its flows terminate, but in reality this rarely happens. That is why we need to make a compromise between the goal of keeping the flows on the same port and having equal traffic distribution within the output ports. This tradeoff is controlled by the *R* parameter and its details are discussed in Section IV.D.

C. Bloom filter selection

The implemented Bloom filter selection algorithm is compliant with the OpenFlow standard. The publicly available BF implementations were re-used and enhanced with the RRBF algorithm.

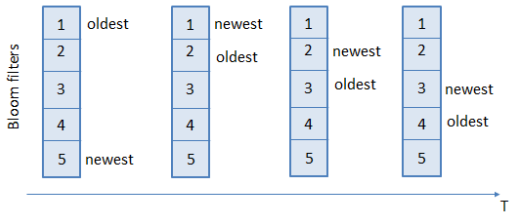

Fig. 3 Shifting of Bloom filters after each *T* period

For each ingress packet, after being matched as an IP packet by the flow entry and passed to the first group entry, we calculate the fingerprint as the XOR of source and destination IP addresses and then we check if it's time to switch to the next youngest filter (see Fig. 3). If not, then we go through all the filters, from oldest to youngest, and do a membership query operation for the given fingerprint. If the fingerprint is present in any of the filters, we select that one; otherwise we do an insert operation to the youngest one. On the other hand, in case the period (*T*) has ended, we clear the oldest filter and recreate it, then shift the youngest filter to the next one and do the same as described above. Each bucket in the first group entry containing a filter, has the same action of forwarding the IP packet to the next group entry.

D. Output port selection

The implementation was designed such as the output port selection supports our load balancing goal. After the IP packet arrives to the second group entry, which has a number of buckets each having an action of forwarding the packet to an output port, it will be sent out on the selected port. Important to know, that after each period (*T*), when the youngest filter is shifted, we also search and select the least loaded port and assign it to the filter. So, at any given time, each filter has a port assigned to it which are continuously sending out packets, then at timeout, the youngest filter might get a new port assigned based on the number of transmitted packets on each port.

E. Startup transient elimination

As introduced in Section I, the startup transient problem must be solved before load balancing solutions can be deployed to support packet flows. Startup transient period is present at the time of connecting (or activating) the load balancer to the network. The input traffic can contain a lot of already active flows, and it is a concern that in the first period (*T*), the youngest filter can be filled with most of the ingress flows, and the system can remain unbalanced, because the first filter will not be cleared until the first epoch (*Ep*) has ended. In practice this means that all incoming flows during the first period (*T*) will be registered in the first youngest filter, and all other filters will remain empty. Therefore the youngest filter may fill up in a short period of time and so the false positive probability can increase significantly. The other issue introduced by the startup transient is that the flows present at the startup of the load balancer will always belong to the same filter. The system will get balanced only after most of the original flows decay, which can take time.

To compensate for this *startup transient* problem, and to make plug and play deployment possible, the startup transient needs to be eliminated. In this paper we propose a solution that for a configurable amount of packets (*Tr*) at the beginning, the system will always rotate the youngest filter, as it would happen at the end of each period (*T*). The Bloom filter selection algorithm will be called for each consecutive packet, assuring that the existing flows will be associated to their original filters, and only the new flows will be stored in the youngest filter.

Rotating the filters at every incoming packet gives the possibility for the incoming flows to be evenly distributed within the filters, ameliorating the effect of the startup phenomenon. The solution can be further enhanced to achieve even better distribution of flows within the filters, e.g. by rotating the youngest filter only if the respective incoming packet was belonging to a new flow. This way we make sure that each filter will register new flows.

IV. EVALUATION OF THE LOAD BALANCER

A. Testing scenario

A set of experiments were conducted with different system parameter combinations to test our proposal. The goal was to prove that the system is performing as expected under real-life traffic scenarios. We simulated the hot deployment scenario by running real-life traffic samples through the system. The publicly available Internet traffic traces were used provided for the research community from the SimpleWeb project [16]. The sample traces contain ~8000 to ~16000 TCP/IP packets per period (*T*), and the ratio of new flows vs. old flows is around 35% to 92% per period (*T*) depending on the period length.

In this paper we illustrate our measurement results using three traffic traces selected from these. Fig. 4 shows the flow distribution of sample trace #1 we use in this paper to explain our design decisions. This trace had a 14534 pckt/sec average packet rate. It can be seen that on average ~65% of the flows in any period (*T*) were already active at least in the previous period (*T-1*), as well. As for trace #2, ~8% of the flows present in a particular period were also present at least in the previous period and the average packet rate was 7804 pckt/sec. Trace #3 was only used for initial tests, conducted to calibrate the N and E parameters. It contains ~1000 flows and ~50% of the flows are longer than 1sec.

When startup transients are eliminated, the *Tr* parameter has a value of 10000, meaning that the first seconds (depending on the actual load) are used only to "initialize" the RRBF.

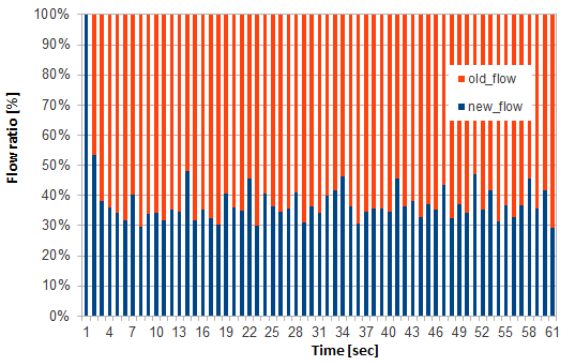

Fig. 4 Ingress flow distribution for trace #1

B. Round Robin Bloom filters without periodical state reset

We evaluate the effectiveness of the load balancing at packet level, because that increased the execution speed of our experiments. This does not affect the generality of our results, because the decision to associate a new port or not to the filter at the beginning of a new period is similar in both cases. The only difference is that instead of counting the number of packets per port, we would have to count the bytes contained within the packet. This would neither increase the granularity of the process.

TABLE 2
EXPERIMENTS WITH DIFFERENT SETTINGS OF THE NUMBER OF EXPECTED FLOWS (*N*) AND FALSE POSITIVE RATE (*E*)

RRBF with two BFs	**N=100, E=0.01%**	**N=1000, E=0.01%**	**N=1000, E=1%**
BF1 egress packets	37547	35652	35499
BF2 egress packets	40943	42838	42991
Egress packets due to false positive membership query	13593	0	1236
BF1 egress flows	637	602	599
BF2 egress flows	310	469	465
Egress flows due to false positive membership query	**124**	**0**	**7**
Total flows	1195	1071	1078

We start with a basic experiment using capture #3 and consisting of two Bloom filters each assigned to a separate output port. We want to examine the flow distribution process, focusing on the false positive rate depending on the BF configuration. After every incoming new flow the roles of the oldest and youngest filters were switched, so that each new flow could be stored in the next filter. Still, the bits of the filters are never reset, preserving the previous state, the memory of the all flows inserted earlier. That is the reason why we refer to these experiments as the ones were the periodical *state reset* was avoided. The results, shown in Table II above, prove that the false positive probability can be influenced by the Bloom filter parameter values. Because the filters were never reset, if the number of expected flows (*N*) was not high enough, false positives started to appear. We counted the number of egress packets and flows where the membership query resulted in false positive matches. This happened in case *N* was lower than the total number of ingress flows, or in case that *E* was too high.

These results confirm that RRBF with the original BF (i.e. without periodical reset of the BF bits) is not working and it is needed the mechanism proposed in [6], indeed.

C. RRBF and startup transients

In this sub-section we illustrate the effect on the original RRBF proposal of the flow transient problem. Based on our experiments we set the main parameters of the RRBF as follows: we used 10 hashes (*K = 10*), the false probability rate was reduced to *E = 0,01%* and the number of elements was set *N = 1000*. These parameters were used in all experiments presented from now on in this paper. The results in this sub-section were obtained by using traffic trace #1.

Fig. 6 shows the number of registered new flows per Bloom filter (*bf_flow N*) in every period (*T*). In the beginning the first

Bloom filter from a RRBF mechanism with five BFs will carry more flows than the other ones, because it "keeps locked in" the long flows and so the flow distribution gets unbalanced. After an epoch has passed the first filter will be the youngest again and it will keep carrying its old flows.

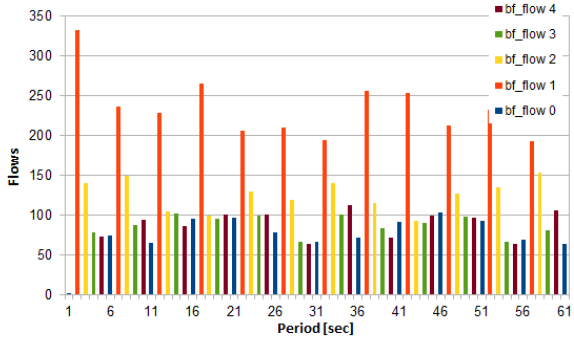

Fig. 5 Flows per Bloom filter with periodical state reset

Note that this impacts the per-packet load balancing performance of the mechanism, as well (Fig. 6). Within each epoch the port associated to the youngest filter will be loaded with the packets of the heaviest flows. Since we have 5 BFs and $T = 1$, the curve breaks at each 5 seconds.

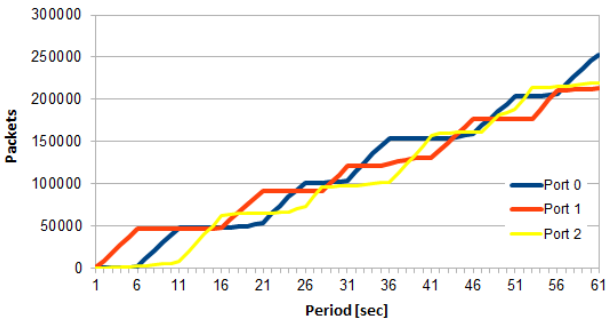

Fig. 6 Packets per output port with periodical state reset

These results illustrate our motivation to handle the transients during the startup.

D. RRBF with elimination of the startup transient

The experiments discussed in this sub-section deploy our solution to eliminate the startup transient phenomenon. For this we used our implementation of the method proposed in Section III. E and traces in Section IV. A. The implementation features the initialization until the first *Tr* packets are received, as described earlier. Additionally, we also use a mechanism that is controlled through the *R* parameter. This mechanism measures the ratio of the incoming packets during the last period *T* and those received during the whole epoch. If it is less than *R*, then we consider that the BF can be associated to a new port (i.e., the least loaded one), otherwise we do not change the association. After several test runs and based on empirical results we set the value of *R* to 10%.

Fig. 7 below shows the number of registered new flows per Bloom filter in every period (*T*). During the first period the incoming flows are evenly distributed within the Bloom filters, and this distribution keeps the system balanced throughout the measurement. Long flows (longer at least than one epoch) are carried by multiple filters.

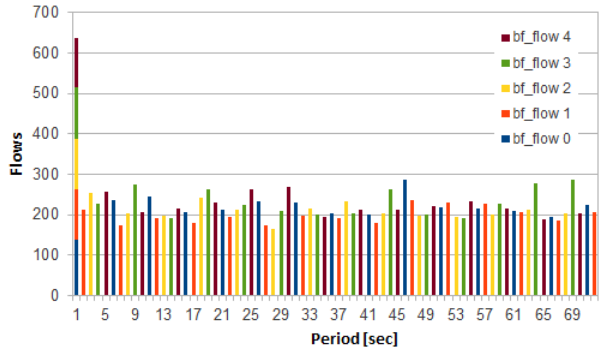

Fig. 7 Flows per Bloom filter with elimination of the startup transients

Applying our proposal also improves the quality of load balancing, as well. As seen in Fig. 8, the number of packets sent over the three ports has more even distribution.

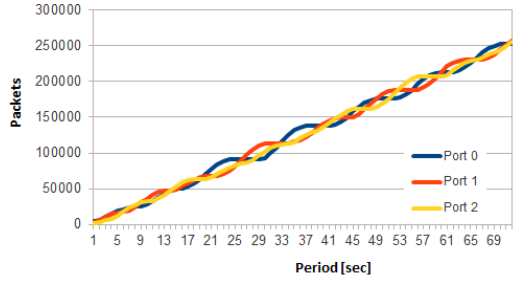

Fig. 8 Packets per output port with elimination of the startup transient

We repeated the experiment using trace #2, as well. The results were similar. Based on the theoretical results we started from this was expected for the flow distribution. But it proved that it works for the load distribution, too, as shown in Fig. 9.

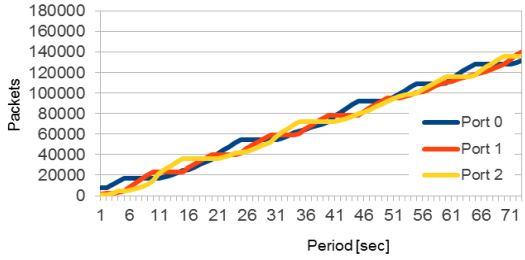

Fig. 9 Packets per port with elimination of the startup transient (trace #2)

Note that by increasing the number of BFs we obtain finer granularity and we can make a balance between the two goals: distribute flows among different ports and evenly distribute the traffic volume. By increasing *R* we have better load balancing,

but this will affect some longer flows, as they might be distributed among several output ports. To remedy that, we can increase the number of filters from 5 to 15, while keeping *R* down at 10%. We run an experiment, where the only change compared to the one analysed in this sub-section above was the use of 15 Bloom filters, and it slightly better balanced the load of the flows. Nevertheless, if there were elephant flows in the traffic mix whose lifetime exceeded the epoch duration, then this change could not fully eliminate the effect of it.

We also tested higher R parameter values (e.g., 30% instead of 10%), which results in more aggressive port selection behavior, leading to better load sharing among the ports. Nevertheless, this affects more often the longer flows, forwarding their packets over different ports.

V. CONCLUSIONS

We designed an OpenFlow compatible flow based load balancer with Round Robin Bloom filters supporting plug and play deployment scenarios. We demonstrated in an emulated SDN environment, using real-life traffic traces that the solution can eliminate the startup transient problem during initialization and the system remains balanced, meaning that the ingress flows are more evenly distributed within the Bloom filters.

Our future plan is to further investigate our solution in more complex traffic conditions. Our main focus will be on separating elephant flows that carry large traffic volumes and have longer duration. We are considering the possibility to deploy separate RRBF systems in parallel and use on-the-fly traffic classification (e.g. short – HTTP, long – video) by controller to feed the different systems with such homogeneous traffic.

ACKNOWLEDGMENT

The authors thank to Robert Szabó for his valuable comments during the implementation work of the Round Robin Bloom filters.

REFERENCES

[1] Cardellini, V., Colajanni, M. and Philip, S.Y., 1999. Dynamic load balancing on web-server systems. IEEE Internet computing, 3(3), p.28-39.

[2] Open Networking Foundation: Software-defined Networking: The new norm for networks, (accessed on April 2016).

[3] Yuanhao Zhou, Li Ruan, Limin Xiao, Rui Liu, "A Method for Load Balancing based on Software Defined Network", Advanced Science and Technology Letters Vol.45 (CCA 2014), pp.43-48.

[4] S. Tarkoma, C. Rothenberg, and E. Lagerspetz, "Theory and Practice of Bloom Filters for Distributed Systems", IEEE Communications Surveys & Tutorials, Vol. 14. no. 1., 2012.

[5] A. Broder and M. Mitzenmacher, "Network applications of bloom filters:A survey," Internet Mathematics, vol. 1, no. 4, pp. 485–509, 2004.

[6] R. Szabó, "A Round-Robin Bloom Filter for Stateful Control over Event Streams", 2013 IEEE 4th International Conference on Cognitive Infocommunications (CogInfoCom), 2013.

[7] K. Cheng, L. Xiang, and M. Iwaihara, "Time-decaying bloom filters for data streams with skewed distributions," in 15th International Workshop on Research Issues in Data Engineering: Stream Data Mining and Applications, 2005. RIDE-SDMA 2005, Apr. 2005, pp. 63–69.

[8] H. Shen and Y. Zhang, "Improved approximate detection of duplicates for data streams over sliding windows," Journal of Computer Science and Technology, vol. 23, no. 6, pp. 973–987, 2008.

[9] Z. Changling, X. Jianguo, C. Jian, Z. Bei, and L. Feng, "Approximate discovery of service nodes by duplicate detection in flows," China Communications, vol. 9, no. 5, pp. 75–89, Jul. 2012. [Online]. Available:
http://www.chinacommunications.cn/EN/abstract/article 7912.shtml

[10] Chengcheng G. et al., „A load-balancing scheme based on Bloom Filters", in. proc. of the IEEE Second International Conference on Future Networks, Washington DC, USA, 2010, pp. 404-407.

[11] Fan L., Cao P., Almeida J., Broder A., "Summary Cache: A Scalable Wide-Area Web Cache Sharing Protocol", IEEE/ACM Transactions on Networking, 8 (3): 281–293, 2000.

[12] Mininet, http://www.mininet.org/, (accessed on April 2016).

[13] CPqD OpenFlow switch: http://cpqd.github.io/ofsoftswitch13/ (accessed on April 2016).

[14] Jyri J. Virkki's Bloom filter: https://github.com/jvirkki/libbloom (accessed on April 2016).

[15] Austin Appleby's MurmurHash2: https://sites.google.com/site/murmurhash/ (accessed on April 2016)

[16] SimpleWeb, http://www.simpleweb.org/wiki/Traces/ http://cpqd.github.io/ofsoftswitch13/ (accessed on April 2016).

Örs Szabó has graduated as an MSc software engineer from the Budapest University of Technology and Economics. During his last student years he worked as a part-time employee in the field of packet-switched voice communication over 4G mobile networks at Ericsson Hungary. Currently he works at the same company as a system engineer.

Csaba Simon is a software engineer and he earned his PhD in 2012 at the Doctoral School of Informatics of the Budapest University of Technology and Economics and currently works as an assistant professor at the Department of Telecommunication and Media Informatics of the same university. His research area includes the topics of Future Internet, 5G networks and cloud systems.

A Novel DOA Estimation Methodology Utilizing Null Steering Antenna Algorithm

Zeeshan Ahmad, Yaoliang Song

***Abstract*—Past decades have seen significant advances in array signal processing and its applications. Direction of Arrival (DOA) estimation is one the most significant application of antenna arrays. This paper presents a new direction-of-arrival (DOA) estimation methodology, where DOA estimation is realized by the nulling antenna algorithm. The new methodology aims to minimize the computational complexity while maintaining high degree of accuracy and resolution. Unlike the existing MUSIC algorithm, the proposed algorithm eliminates the need of estimating the number of signals and the eigenvalue decomposition of covariance matrix, thereby avoiding performance deterioration caused by incorrect source number estimation. Both the theoretical analysis and computer simulations show that the proposed method outperforms the conventional techniques in estimating DOA of signals while having less computational complexity and high resolution.**

***Index Terms*—DOA Estimation, Adaptive Filtering, Spatial Filtering, Power Inversion, Array Signal Processing.**

I. INTRODUCTION

DOA estimation is a prominent figure in the field of array signal processing applied in satellite navigation systems, radars, sonars, seismic and mobile communication systems [1-3]. The principal thrust of the research in array signal processing over the last decade has been directed towards DOA estimation. The reason behind this widespread interest is the motivation by the tremendous popularity of the null steering antenna, which emerged as a key technology to accomplish the striving requirement of enhanced range and capacity [1-5].

There are many applications where the sole focus is the precise estimation of a signals direction of arrival (DOA). Radar, sonar, and mobile communication systems are not all but few examples of many possible applications. DOA methods are utilized for designing and adapting of the directivity of antenna arrays. For example, an antenna array can be designed to accept signals from some specific directions, while rejecting signals from all other directions by declaring them as interference. [6]

In lots of DOA estimation algorithms with excellent performance, MUSIC is one of the leading super resolution algorithm that has attracted attention in past two decades [7-8]. However, due to the fact that MUSIC algorithm needs the estimate of the number of sources and the Eigen-value decomposition of the covariance matrix of the received signal, the implementation of these operations in FPGA or DSP devices are more difficult and expensive [9-10]. So a new algorithm has been derived to achieve DOA estimation utilizing null steering antenna and spatial filtering algorithm to eradicate the limitations in MUSIC algorithm. The new algorithm works well for any kind of geometry of antenna array.

The remaining paper is structured as follows. Section 2 introduces the basic concept of nulling antenna in adaptive filtering by elaborating on the signal model and adaptive filtering algorithm. Section 3 covers the proposed methodology of DOA estimation algorithm based on adaptive filtering. Section 4 discusses the performance analysis of the proposed algorithm in detail. The simulation results of the proposed algorithm are given in section 5. Finally section 6 offers some conclusions drawn on the basis of simulation results.

II. NARROWBAND NULL STEERING

The two basic approaches to spatial filtering that are directly applicable to Direct Sequence Spread Spectrum (DSSS) systems are null Steering and beamforming. Null steering approaches require minimal knowledge of the desired signal and are generally easier to implement than beamforming.

Narrowband null steering is the simplest spatial filtering approach. The basic idea is to simply place nulls in the direction of the interference signals. This approach is depicted in Fig. 1:

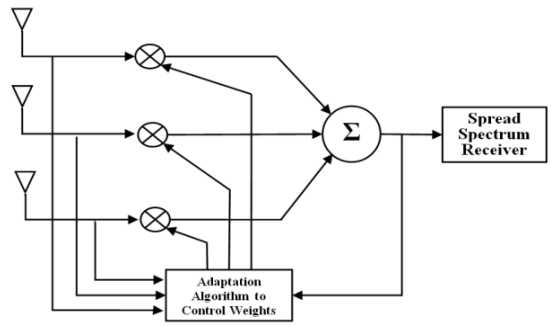

Fig. 1. Narrowband Null Steering.

The authors gracefully acknowledge the support of the National Natural Science Foundation (NSFC) Project (61271331) and project (61071145) of China.

The authors are with the School of Electronic Engineering & Optoelectronic Technology, Nanjing University of Science & Technology, Nanjing (210094), Jiangsu Province, P.R.China (e-mail: engr.zeeshan@hotmail.com, ylsong@njust.edu.cn).

The antenna pattern typically is initially configured as an omni-directional pattern. Other initial patterns are possible and are determined by the initial beam steering vector. For example, the initial beam steering vector may be configured to mask off low elevation angles and jammers generally arriving from lower elevation angles. The adaptive algorithm modifies the complex antenna weights to minimize the power at the output of the antenna summing junction. This results in nulls in the antenna pattern in the direction of the undesired signals provided that jamming signal is stronger than the desired signal. This approach works best when the desired signal is well below the noise floor. If the desired signal is not well below the noise floor, this approach would null the desired signal. For many DSSS systems this is not an issue since the DSSS signal is well below the noise floor. Compton gives an excellent example of this approach in [11]. This method can be also used for DOA estimation to cop up the shortcomings of the MUSIC algorithm and classical Delay-and-Sum method.

A. Signal Model

Assume a uniform linear array (ULA) with N+1 elements, where the first 0-based array element is located at the origin of the coordinates, and the remaining N elements represents auxiliary array. Let the signal incident on the main array element represent the reference signal which is given by:

$$x_0(k) \quad s_0(k) \quad \sum_{m=1}^{M} s_m(k) \quad n_0(k) \tag{1}$$

where $s_0(k)$ is the desired signal, $s_m(k)$ are the M interference signals, given that $m \quad 1,2,3,\cdots,M$ and $n_0(k)$ is the noise. Assuming that the interference signal and desired signal are narrowband signals at the same frequency and the spacing between the adjacent elements of the array is half-a-wavelength, the signal received at the auxiliary array is:

$$\boldsymbol{x}(k) \quad \begin{bmatrix} x_1(k) \\ \vdots \\ x_N(k) \end{bmatrix} \quad s_0(k)\upsilon(\quad_0) \quad \sum_{m=1}^{M} s_m(k)\upsilon(\quad_m) \quad \boldsymbol{n}(k) \tag{2}$$

where $\upsilon(\quad_0)$ and $\upsilon(\quad_m)$ are the array steering vectors of the desired and m-th interference signal respectively, which depend on the values of the DOA $\quad_0$ and $\quad_m$ of the desired and interference signals.

In fact, the desired signal conducted by the null steering antenna is weak and the wireless environment such as the satellite navigation system experiences strong signal interference. The desired signal due to the impact of spread spectrum modulation in the above received signal model is far less than the noise [12]. Therefore, (1) can be simplified to:

$$x_0(k) \quad \sum_{m=1}^{M} s_m(k)\upsilon(\quad_m) \quad \boldsymbol{n}_0(k) \tag{3}$$

Consider the vector array of the signal model:

$$\boldsymbol{x}(k) \quad \begin{bmatrix} x_1(k) \\ \vdots \\ x_N(k) \end{bmatrix} \quad \sum_{m=1}^{M} s_m(k)\upsilon(\quad_m) \quad \boldsymbol{n}(k) \tag{4}$$

B. Adaptive Filtering Algorithm

In satellite navigation applications, power inversion adaptive filtering method has the configuration shown in Fig. 2 [13]. The main array element receives a signal $x_0(k)$ as the reference signal while the auxiliary array element receives a signal $\boldsymbol{x}(k)$ using the power inversion criterion [14], in order to get the least mean square error between the weighted sum of the signal and the reference signal, which is called the cost function:

$$J(\boldsymbol{w}) \quad E[e(k)e \ (k)] \tag{5}$$

which has a minimum value, where the error $e(k)$ is defined as:

$$e(k) \quad x_0(k) \quad \boldsymbol{w}^H(k)\boldsymbol{x}(k) \tag{6}$$

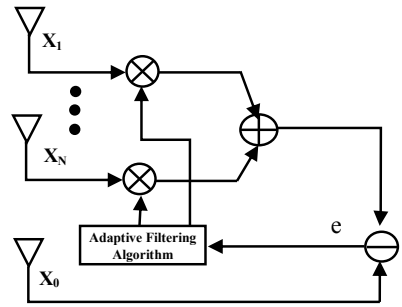

Fig. 2. Structure of spatial filter

According to the study of basic theory of adaptive filtering [15], the optimal (Wiener) solution is given by

$$\boldsymbol{w}_{opt} \quad \boldsymbol{R}^{\ 1}\boldsymbol{p} \tag{7}$$

where

$$\boldsymbol{R} \quad E[\boldsymbol{x}(k)\boldsymbol{x}^H(k)] \quad \sum_{m=1}^{M} \quad _m^2\upsilon(\quad_m)\upsilon^H(\quad_m) \quad \quad _n^2\boldsymbol{I} \tag{8}$$

$$\boldsymbol{p} \quad [\boldsymbol{x}(k)x_0(k)] \quad \sum_{m=1}^{M} \quad _m^2\upsilon(\quad_m) \tag{9}$$

$\boldsymbol{R}$ is the covariance matrix of the received signal, $\boldsymbol{p}$ is cross-correlation vector of the received signal with the reference signal, $\quad_m^2$ is the power of m-th interference signal, and $\quad_n^2$ is the noise power.

In the LMS algorithm, the covariance matrix ($\boldsymbol{R}$) and the cross correlation vector ($\boldsymbol{p}$) are replaced by their instantaneous values.

In the Wiener solution case, the minimum mean square error is given by:

$$J_{\min} \quad J(\boldsymbol{w}_{opt}) \quad \quad_0^2 \quad \boldsymbol{p}^H\boldsymbol{R}^{\ 1}\boldsymbol{p} \tag{10}$$

where, $\quad_0^2$ is power of reference signal.

In case of using LMS algorithm [16], weighted iteration method is:

$$e(k) \quad x_0(k) \quad \boldsymbol{w}^H(k)\boldsymbol{x}(k) \tag{11}$$

$$w(k \quad 1) \quad w(k) \quad \quad \boldsymbol{x}(k)e \ (k) \tag{12}$$

The basic idea of the above algorithms is that, if the interference signal have a larger interference-noise ratio, and

the desired signal is small, the error $e(n)$ is the output signal after interference is been eliminated. Consider all N+1 elements as a new antenna array, and $e(n)$ is the output signal of the system, the weight vector and the direction vector are equivalent to:

$$\boldsymbol{w}_e = \begin{bmatrix} 1 \\ \boldsymbol{w} \end{bmatrix} \tag{13}$$

$$\upsilon_e(Z) = \begin{bmatrix} 1 \\ \upsilon(Z) \end{bmatrix} \tag{14}$$

After convergence of the weight vector based on the adaptive filter theory, the array Pattern is:

$$B(\Box) = \boldsymbol{w}_e^H \upsilon(Z) \tag{15}$$

Since the input signal consist of only interference and noise, so it form nulls in the spatial spectrum which only appears in the interfered DOA zone, while the remaining angles are relatively flat.

III. Proposed Methodology

The DOA's of multiple incident signals can be estimated according to the preceding section, which introduces the adaptive spatial filtering based on nulling antenna. Use iterative equations (11) and (12) to compute the weight vector until the algorithm is converged. The new weight vector is formed according to (13). The convergence factor P used in (12) should be chosen in a specific range to guarantee convergence of the weight vector. This is discussed briefly in the upcoming sections.

According to (15) nulls are placed in the DOA of signals only, so the spatial spectrum for DOA estimation can be defined as a reciprocal of (15) and can be defined as:

$$P(Z) = \frac{1}{|B(Z)|} = \frac{1}{\boldsymbol{w}_e^H \upsilon_e(Z)} \tag{16}$$

Clearly, the nulls in the reciprocal of spatial spectrum will appear as spectral peaks and peak positions are the estimated DOA of the signal.

Thus, the proposed DOA estimation algorithm does not require a prior estimation of the number of sources, which avoid performance degradation when the numbers of sources are over-estimated or under-estimated as in MUSIC algorithm. Moreover, the computational complex process of Eigen-value decomposition is also eliminated in case of proposed algorithm.

The implementation of the proposed algorithm is summarized as follows.

TABLE I
SUMMARY OF THE PROPOSED ALGORITHM

Implementation steps of proposed algorithm	
1)	*Parameters*: N = number of sensors μ= step-size $0 < \mu < \frac{2}{\lambda_{max}}$ where λ_{max} is the maximum eigenvalue of $\boldsymbol{R}$.
2)	*Initialization*. If prior knowledge about the weight vector $\boldsymbol{w}(k)$ is available, use that knowledge to select an appropriate value for $\boldsymbol{w}(0)$. Otherwise, set $\boldsymbol{w}(0) = 0$.
3)	*Data* Given: $x_n(k)$ = N+1-by-1 tap input vector at time k, where $n = 0,1,\ldots,N$ $x_0(k)$ = reference signal.
4)	To be computed: $\boldsymbol{w}(k+1)$ = estimate of tap-weight vector at time step $k + 1$. *Computation*: For $k = 0, 1, 2, \ldots$, compute $e(k) = x_0(k) - \boldsymbol{w}^H(k)\boldsymbol{x}(k)$, $w(k+1) = w(k) + \mu x(k) e^*(k)$.
5)	Form a new weight vector $\boldsymbol{w}_e$ according to equation (13);
6)	Compute the spatial spectrum based on (16).

IV. Performance Analysis

A. Stability Analysis

Stability of the LMS algorithm is an important performance metric. Here, we analyze the conditions for the stability of the LMS algorithm. The close form for the MSE learning curve of the LMS algorithm for small P can be expressed as [17]:

$$\begin{aligned} J(k) &= J_{min} + PJ_{min}\sum_{n=1}^{N}\frac{\lambda_n}{2-P\lambda_n} \\ &+ \sum_{n=1}^{N}\lambda_n\left|\upsilon_n(0)\right|^2\left(1-P\lambda_n\right)^{2k} - \frac{PJ_{min}}{2-P\lambda_n} \end{aligned} \tag{17}$$

where λ_n is the $n-th$ eigenvalue of the covariance matrix $\boldsymbol{R}$, and $\upsilon_n(k)$ is the instantaneous covariance matrix and the error determines the instantaneous value of the weight vector [18].

Equation (17) represent the mean-square error produced by the LMS algorithm for small P compared to the permissible limit $2/\lambda_{max}$.

Equation (18) gives the sufficient condition for the convergence of the proposed algorithm, which is the value of the step size P and it should be:

$$0 < P < \frac{2}{\lambda_{max}} \tag{18}$$

This condition does not ensure the stability of the LMS algorithm, instead it guarantees the convergence of the algorithm. The MSE does not exactly converge to J_{min} due to the oscillations. To characterize this property in steady state, a new measurement referred to as the misadjustment for small P is defined as

$$\mathcal{M}=\frac{\sum_{n=0}^{N-1}\frac{P\lambda_n}{1-2P\lambda_n}}{1-\sum_{n=0}^{N-1}\frac{P\lambda_n}{1-2P\lambda_n}} \tag{19}$$

Where

$$\sum_{n=0}^{N-1}\frac{P\lambda_n}{1-2P\lambda_n}=\sum_{n=0}^{N-1}P_n=P\mathrm{Tr}(\boldsymbol{R}) \tag{20}$$

So we get

$$\mathcal{M}=\frac{P\mathrm{Tr}(\boldsymbol{R})}{1-P\mathrm{Tr}(\boldsymbol{R})} \tag{21}$$

When $\mathcal{M}$ is sufficiently small, $P\mathrm{Tr}(\boldsymbol{R})$ can be ignored it in the denominator in order to obtain

$$\mathcal{M}=P\mathrm{Tr}(\boldsymbol{R}) \tag{22}$$

This new refined formula predicts the misadjustment more accurately. For small values of P, it is identical to the original formula.

From the above analysis we can conclude that the step-size parameter governs the convergence speed of the LMS algorithm. Large step-size P speeds up the convergence of the algorithm, while it reduces the precision of the steady-state solution of the algorithm as from (22). Therefore, the algorithm has a trade-off between the convergence speed and the misadjustment.

B. Computational complexity

Computational complexity of the proposed algorithm comprises of the iterative calculations of the weight vector and the spatial spectrum calculation. Eq. (17) shows that the evolution of the mean-square error is governed by the exponential factor $(1-P\lambda_n)^{2k}$. If the time constant W is used to define the number of iterations required for the amplitude of $J(k)$ to decay to $1/e$ of its initial value, we can approximate W for small P as

$$W\approx\frac{-1}{2\ln(1-P\lambda_{\min})} \tag{23}$$

Therefore, the LMS algorithm has N time constants corresponding to its N eigenvalues. The exponential factors corresponding to large eigenvalues decrease to zero fast, whereas small eigenvalues slow down the overall convergence.

The algorithm weights are updated according to (11) and (12), each iteration requires two times complex multiplication and addition respectively, so the number of multiplications and additions is defined as:

$$2W\approx\frac{-1}{\ln(1-P\lambda_{\min})}\approx\frac{1}{P\lambda_{\min}} \tag{24}$$

While in computation of spatial spectrum, each search angle will be calculated by equation (16). Since the first element in the weight vector and the direction vector is a constant 1, so one iteration of the proposed algorithm requires N multiplications and N additions for the weight updating and error generation. The number of computations depends on the search step , then for linear array the number of computations requires to estimate the spatial spectrum is $\approx N/S$.

Combining the two computations, multiple numbers of multiplications and additions required by the algorithm is $\frac{1}{P\lambda_{\min}}\approx\frac{SN}{\approx T}$.

In contrast to MUSIC algorithm, the proposed algorithm requires iterative computations, which makes it less complex. On the other hand, the MUSIC algorithm performs the eigen-decomposition of the covariance matrix and also requires the estimate of the number of sources. These operations make the MUSIC algorithm more complex and hard to implement in real-time applications.

C. Error estimation

The ensemble-average learning curve of the LMS algorithm does not exhibit oscillations, rather it decays exponentially to the constant value. When the number of iterations tends to infinity, the third term is zero in (17) and the error of the filter is equal to

$$J(\infty)\approx J_{\min}+\sum_{n=1}^{N}\frac{P\lambda_n J_{\min}}{2-P\lambda_n} \tag{25}$$

$$J(\infty)\approx J_{\min}\left(1+\sum_{n=1}^{N}\frac{\lambda_n}{2-P\lambda_n}\right)\approx J_{\min}+P \tag{26}$$

Whereas, the signal and noise power determine the characteristic value, i.e.

$$\lambda_n=\begin{cases}\sigma_m^2+\sigma_n^2, n=m=1,2,\cdots,M\\ \sigma_n^2, n=M+1,\cdots,N\end{cases} \tag{27}$$

For small step size, the MSE is given by

$$\xi(\infty)\approx\frac{NP\sigma_n^2}{2}+\sum_{m=1}^{M}\frac{\sigma_m^2}{2} \tag{28}$$

The inverse of covariance matrix in (8) by matrix inversion can be derived as

$$\boldsymbol{R}^{-1}=\frac{1}{\sigma_n^2}\boldsymbol{I}-\frac{1}{\sigma_n^2}\sum_{m=1}^{M}\frac{\sigma_m^2}{N\sigma_m^2+\sigma_n^2}\upsilon(\theta_m)\upsilon^H(\theta_m) \tag{29}$$

Substituting (9) and (29) into (10) and considering the spatial orthogonality between the signals produces:

$$J_{\min}=\sigma_0^2-\mathbf{p}^H\mathbf{R}^{-1}\mathbf{p}=\sigma_n^2-\sum_{m=1}^{M}\frac{N\sigma_m^4+2\sigma_m^2\sigma_n^2}{N\sigma_m^2+\sigma_n^2}$$
$$=\sigma_n^2-\sum_{m=1}^{M}\frac{\sigma_m^2}{N\frac{\sigma_m^2}{\sigma_n^2}+1} \tag{30}$$

Equations (28) and (30) show that the array output error in the LMS algorithm increases as the signal power or the noise power increases, while the output error can be reduced by enhancing the SNR.

D. Resolution Performance

Since the optimal weight vector is theoretically equal to the Wiener solution, the spatial spectrum can be expressed by substituting (7) into equation (16) as:

$$p(\theta) = \left| \frac{1}{1 - \mathbf{p}^H \mathbf{R}^{-1} \mathbf{v}(\theta)} \right| \quad (31)$$

For any two spatial incident signals θ_{m1} and θ_{m2}, the condition for distinguishing is given as:

$$p\left(\frac{\theta_{m1} + \theta_{m2}}{2}\right) > p(\theta_{m1}) \quad (32)$$

Let $\sigma_{m1}^2 = \sigma_{m2}^2$, then:

$$\mathbf{p}^H \mathbf{R}^{-1} = \sum_{i=1}^{M} \frac{\sigma_{mi}^2}{N\sigma_{mi}^2 + \sigma_n^2} \mathbf{v}^H(\theta_{mi}) \quad (33)$$

Inequality is

$$\sum_{i=1}^{2} \frac{\sigma_{mi}^2}{N\sigma_{mi}^2 + \sigma_n^2} \mathbf{v}^H(\theta_{mi}) \mathbf{v}(\theta_{m1}) > \frac{\sigma_{m1}^2}{2} > \frac{N\sigma_{m2}^2}{N\sigma_{m2}^2 + \sigma_n^2} \quad (34)$$

Since the array steering vector is defined as:

$$\mathbf{v}^H(\theta) = [e^{j\cdot\sin\theta}, \cdots e^{jN\cdot\sin\theta}] \quad (35)$$

Substituting inequality, we have:

$$\left|1 - pa - qa^H\right| > \left|1 - pb - qN\right| \quad (36)$$

where

$$p = \frac{\sigma_{m1}^2}{N\sigma_{m1}^2 + \sigma_n^2} \quad (37)$$

$$q = \frac{\sigma_{m2}^2}{N\sigma_{m2}^2 + \sigma_n^2} \quad (38)$$

$$a = \sum_{n=1}^{N} e^{jn\cdot[\sin\theta_{m1} - \sin(\theta_{m1} - \frac{\theta_{m1}}{2})]} \quad (39)$$

$$b = \sum_{n=1}^{N} e^{jn\cdot[\sin\theta_{m1} - \sin(\theta_{m1} - \theta_{m1})]} \quad (40)$$

Although, the analytical solution of above inequality cannot be calculated, one can get any resolution value under certain conditions through computer programming.

V. SIMULATION RESULTS

In this section, we devise several simulation scenarios to verify the validity of the proposed algorithm. The error estimation and convergence behavior of the proposed algorithm under different step-sizes and SNRs are deeply studied. We also compare the proposed algorithm with the MUSIC algorithm.

A. Impact of SNR on the convergence and DOA estimation of the proposed algorithm

In this simulation, we assume a ULA with eight half-wavelength spaced sensors. One narrowband source with fixed step size P=0.00002 is assumed to impinge the array from $\theta_1 = 30$. The effect of the SNR on the DOA estimation and convergence is analyzed in this scenario. Fig. 3 shows the MSE along the iterations for three different SNRs, estimated from the ensemble-average of 500 independent runs.

It is observed from the MSE learning curve in Fig. 3 that as the SNR increases, the convergence become faster. The convergence time is about 25 iterations when SNR=30 dB, while it take about 150 iterations to converge when SNR=20 dB and for SNR=10 dB, it converges in about 500 iterations. So, convergence rate is directly proportional to SNR.

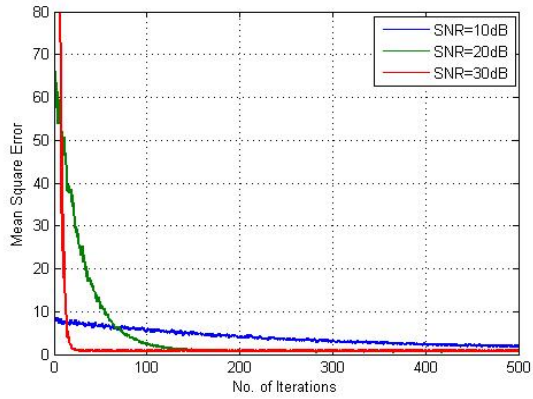

Fig. 3. The output Error curve under constant step.

Fig. 4 shows the spatial spectrum of the proposed algorithm reflects the relationship between $P(\theta)$ and SNR.

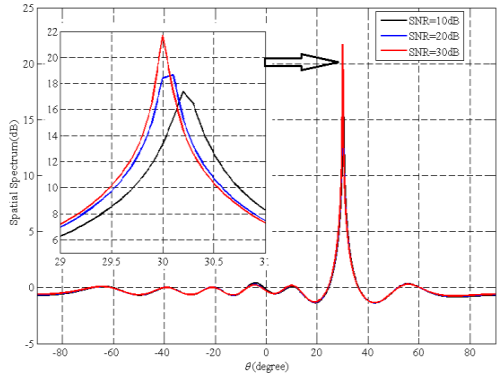

Fig. 4. The corresponding space spectrum under different SNRs.

Fig. 4 shows the spatial spectrum of the signal for $\theta \in [-90, 90]$ and the zoom-part for interval $\theta \in [29, 31]$. From the spatial spectrum of the Fig. 4, it is observed that as the SNR increases, the DOA estimation error decreases and the resolution is improved.

B. Impact of step-size on the convergence time and DOA estimation on the proposed algorithm

Assume the identical scenario as above, the signal impinges on the array from the direction $\theta_1 = 60$, with fixed SNR=20 dB, and different iteration steps μ. The impact of step size on the DOA estimation is analyzed. Fig. 5 shows the MSE along the iterations for three different step-sizes, estimated from the ensemble-average of 500 independent runs.

Fig. 5 is the MSE learning curve that reveals the relationship between the convergence speed and step-size. For smallest step size, the convergence is the slowest. The convergence time is about 300 iterations for μ=0.01/1000. For large step size, μ= 0.01/100, the convergence is the fastest with only 25 iterations. Large step-sizes speed up the convergence of the algorithm, but

also lower the precision of the steady-state solution of the algorithm. This effect can be seen in Fig. 6 given below. In-depth analysis of this behavior is briefly analyzed in the previous sections.

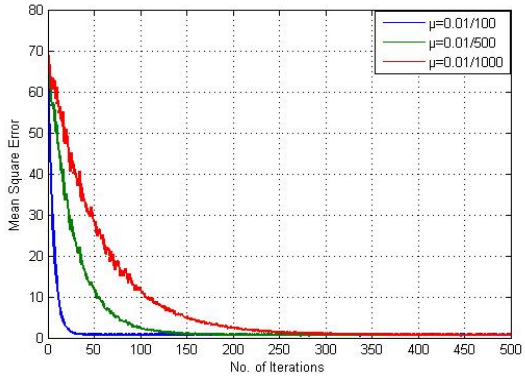

Fig. 5. The output Error curve under constant SNR.

Fig. 6 shows the spatial spectrum of the signal for $\theta \in [-90, 90]$ and the zoom-part for interval $\theta \in [58, 62]$. From the spatial spectrum of the Fig. 6, it can be observed that smaller the step size μ, DOA estimation error is smaller and higher will be the resolution.

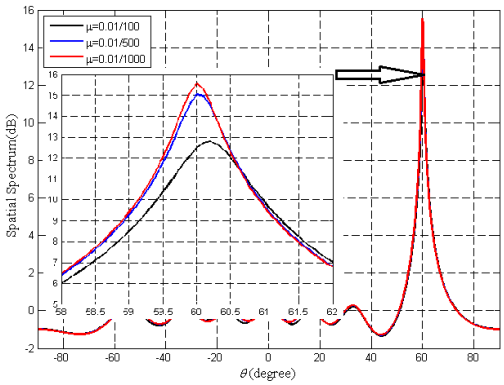

Fig. 6. The corresponding space spectrum under different steps.

C. Comparison with the MUSIC algorithm

In this simulation, we assume a ULA with eight half-wavelength spaced sensors. We evaluate the performance of the algorithms when two narrowband sources are assumed to impinge the array from 30° and 60°. The SNR is set to 10 dB for the target from 30°, and 20 dB for the one from 60°.

Fig. 7 shows the spatial spectrum of the proposed algorithm and the MUSIC algorithm. It can be seen from the figure that both the proposed and the MUSIC algorithms accurately locate the targets. The result shows that, for a large SNR signal of 60°, the peak is high and the resolution is more. It is also observed that the two algorithms achieve similar performance. The performance of the proposed algorithm approaches the MUSIC algorithm when SNR equals 10 dB (for 30° DOA case) in terms of resolution and accuracy. Moreover, when SNR equals 20 dB (for 60° DOA) , the narrow peak of the proposed algorithm slightly outperforms the MUSIC algorithm by yielding narrow peak as compared to MUSIC algorithm.

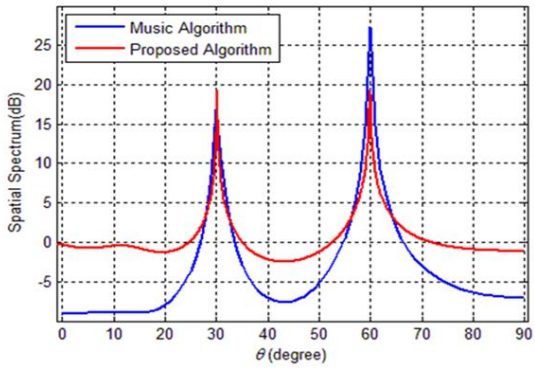

Fig. 7. Comparison of proposed algorithm with the MUSIC algorithm

To further illustrate the superiority of the proposed algorithm when the separation distance between sources is small, we do the following simulation. Consider the identical array condition as previously, the two narrowband sources with DOA 30° and 45° strike a ULA with eight half-wavelength spaced sensors. Fig. 8 shows the spatial spectrum for this scenario. It is observed that both algorithms estimate the DOA for two signals accurately even if the angle separation between signals is smaller.

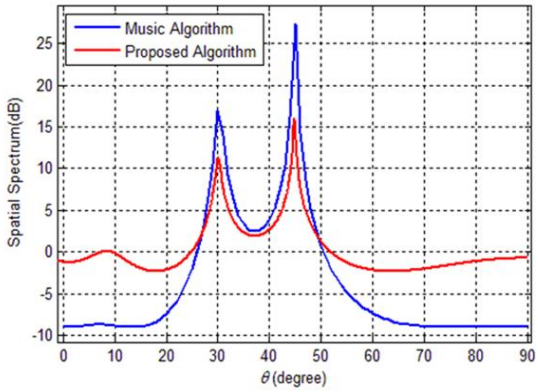

Fig. 8. Comparison of proposed algorithm with the MUSIC algorithm when the two sources lie close to each other

VI. CONCLUSION

A new algorithm for estimating direction-of-arrival (DOA) has been proposed in this paper. The new algorithm achieves DOA estimation utilizing the nulling antenna algorithm. Simulations show the simplicity and accuracy of the proposed methodology. Analysis of results shows that by a careful selection of the step-size, both the accuracy and resolution can be further improved. Compared with the MUSIC algorithm, the new algorithm eliminates the need of source number estimation and decomposition of covariance matrix, thus making the new algorithm less computational complex. Moreover, the proposed

algorithm maintains high resolution in a very elegant and simple manner along with sustaining the distinctive feature of low computational complexity.

REFERENCES

[1] Ahmed Magdy, K. R. Mahmoud, S. G. Abdel-Gawad, and I. I. Ibrahim. Direction of Arrival Estimation Based on Maximum Likelihood Criteria Using Gravitational Search Algorithm,*PIERS Proceedings*, Taipei, 2013.

[2] Ying Zhang; Boon Poh Ng, "MUSIC-Like DOA Estimation Without Estimating the Number of Sources," *Signal Processing, IEEE Transactions on* , vol.58, no.3, pp.1668,1676, March 2010

[3] Robert A. Monzingo, Thomas W. Miller, "*Introduction to Adaptive Arrays*", SciTech Publishing, 1980.

[4] Xiaofei Zhang; Xin Gao; Dazhuan Xu, "Multi-Invariance ESPRIT-Based Blind DOA Estimation for MC-CDMA With an Antenna Array," *Vehicular Technology, IEEE Transactions on* , vol.58, no.8, pp.4686,4690, Oct. 2009

[5] Varade, S.W.; Kulat, K.D., "Robust Algorithms for DOA Estimation and Adaptive Beamforming for Smart Antenna Application," *Emerging Trends in Engineering and Technology (ICETET), 2009 2nd International Conference on* , vol., no., pp.1195,1200, 16-18 Dec. 2009

[6] Jeffrey Foutz, Andreas Spanias, Mahesh K. Banavar. Narrowband Direction of Arrival Estimation for Antenna Arrays. Morgan & Claypool Publishers, 2008

[7] Schmidt, R.O., "Multiple emitter location and signal parameter estimation," *Antennas and Propagation, IEEE Transactions on* , vol.34, no.3, pp.276,280, Mar 1986

[8] Steinwandt, Jens; Roemer, Florian; Haardt, Martin, "Performance analysis of ESPRIT-type algorithms for non-circular sources," *Acoustics, Speech and Signal Processing (ICASSP), 2013 IEEE International Conference on* , vol., no., pp.3986,3990, 26-31 May 2013

[9] Santiago, E.A.; Saquib, M., "Noise Subspace-Based Iterative Technique for Direction Finding," *Aerospace and Electronic Systems, IEEE Transactions on* , vol.49, no.4, pp.2281,2295, OCTOBER 2013

[10] Xuan Li, Xiaochuan Ma, Shefeng Yan, ChaohuanHou, Single snapshot DOA estimation by compressive sampling, Applied Acoustics, Volume 74, Issue 7, July 2013, Pages 926-930.

[11] Compton, R.T., Jr. The Power-Inversion Adaptive Array: Concept and Performance. *IEEE Transactions on Aerospace and Electronic Systems (AES)*, 1979, 15(6): 803-814.

[12] Liu, W.; Zhai, C.R.; Zhan, X.Q.; Zhang, Y.H., "Assessment and analysis of radio frequency compatibility among several global navigation satellite systems," *Radar, Sonar & Navigation, IET* , vol.5, no.2, pp.128,136, Feb. 2011

[13] S.Haykin, Adaptive Filter Theory (3rd ed.), Prentice Hall, Inc., Upper Saddle River, NJ, 1996

[14] Meng, Dawei; Feng, Zhenming; Lu, Mingquan, "Anti-jamming with adaptive arrays utilizing
power inversion algorithm," *Tsinghua Science and Technology* , vol.13, no.6, pp.796,799, Dec. 2008

[15] Ikuma, T.; Beex, A.A.; Zeidler, J.R., "Non-Wiener Mean Weight Behavior of LMS Transversal Equalizers With Sinusoidal Interference," *Signal Processing, IEEE Transactions on* , vol.56, no.9, pp.4521,4525, Sept. 2008

[16] Srar, J.A.; Kah-Seng Chung; Mansour, A., "Adaptive Array Beamforming Using a Combined LMS-LMS Algorithm," *Antennas and Propagation, IEEE Transactions on* , vol.58, no.11, pp.3545,3557, Nov. 2010

[17] Took, C.C.; Mandic, D.P., "The Quaternion LMS Algorithm for Adaptive Filtering of Hypercomplex Processes," *Signal Processing, IEEE Transactions on* , vol.57, no.4, pp.1316,1327, April 2009

[18] Zhang Xiaofei; Lv Wen; Shi Ying; Zhao Ruina; Xu Dazhuan, "A Novel DOA estimation Algorithm Based on Eigen Space," *Microwave, Antenna, Propagation and EMC Technologies for Wireless Communications, 2007 International Symposium on* , vol., no., pp.551,554, 16-17 Aug. 2007

Zeeshan Ahmad was born in Pakistan in 1988. He received the B.E. degree in electrical (telecom) engineering from Bahria University Islamabad, Pakistan, in 2011 and the M.E. degree in electronics and communication engineering from Chongqing University, Chongqing, China, in 2014. Currently, he is enrolled in Nanjing University of Science & Technology, Nanjing, Jiangsu Province, China as a Ph.D Student.
His research interests include array signal processing, radars, beamforming, DOA estimation, communication systems and digital signal processing.

Yaoliang Song was born in Wuxi, China, on June 30, 1960. He received the B.Eng, the M.Eng. and the Ph.D degrees in Electrical Engineering from Nanjing University of Science and Technology, China, in 1983, 1986, and 2000 respectively.
From Sept. 2004 to Sept 2005, he was a Researcher Fellow with the Department of Engineering Science at the University of Oxford. He is currently a Professor at Nanjing University of Science and Technology, and is heading the UWB Radar Imaging Group. His research interests include UWB communication, UWB Radar Imaging, and advanced signal processing.

Editor's Note: IEEE Communications Society has a Sister Society agreement with HTE (The Scientific Association for Infocommunications, Hungary).
The terms of the agreement include re-publication of articles of IEEE Communications Society publications in HTE's Infocommunications Journal.
The article below has already appeared in IEEE Communications Magazine.
The citation is: IEEE Commun. Mag. vol. 53, no. 12, 2015, pp. 64-70.

Enhancements of V2X Communication in Support of Cooperative Autonomous Driving

Laurens Hobert, Andreas Festag, Ignacio Llatser, Luciano Altomare, Filippo Visintainer, and Andras Kovacs

ABSTRACT

Two emerging technologies in the automotive domain are autonomous vehicles and V2X communication. Even though these technologies are usually considered separately, their combination enables two key cooperative features: sensing and maneuvering. Cooperative sensing allows vehicles to exchange information gathered from local sensors. Cooperative maneuvering permits inter-vehicle coordination of maneuvers. These features enable the creation of cooperative autonomous vehicles, which may greatly improve traffic safety, efficiency, and driver comfort. The first generation V2X communication systems with the corresponding standards, such as Release 1 from ETSI, have been designed mainly for driver warning applications in the context of road safety and traffic efficiency, and do not target use cases for autonomous driving. This article presents the design of core functionalities for cooperative autonomous driving and addresses the required evolution of communication standards in order to support a selected number of autonomous driving use cases. The article describes the targeted use cases, identifies their communication requirements, and analyzes the current V2X communication standards from ETSI for missing features. The result is a set of specifications for the amendment and extension of the standards in support of cooperative autonomous driving.

Laurens Hobert is with Hitachi Europe.

Andreas Festag and Ignacio Llatser are with Technische Universität Dresden.

Luciano Altomare and Filippo Visintainer are with Centro Ricerche Fiat.

Andras Kovacs is with Broadbit.

[1] http://www.gcdc.net/i-game

[2] http://www.adaptive-ip.eu

[3] http://www.companion-project.eu

INTRODUCTION

In the last years, there has been tremendous interest in the development of vehicles capable of driving autonomously, from both the research community and industry. Autonomous vehicles promise highly increased traffic safety and fuel efficiency, better use of the infrastructure, and the liberation of drivers to perform other tasks. For these reasons, autonomous driving may create a paradigm shift in the way people and goods are transported.

Most autonomous vehicles currently in development are based on a perception subsystem consisting of onboard sensors, which build a map of the vehicle's environment, and a control subsystem that governs the longitudinal and lateral motion of the vehicle [1–3]. Even though this approach has already been demonstrated in field tests, it presents some drawbacks: first, the limited perception range of onboard sensors only allows for detecting adjacent vehicles; and second, the vehicles are unable to cooperate in order to efficiently perform maneuvers with a high complexity.

These limitations may be overcome by means of vehicle-to-vehicle/infrastructure (V2X) communication, which enables two key features in autonomous vehicles: *cooperative sensing* increases the sensing range by means of the mutual exchange of sensed data, and *cooperative maneuvering* enables a group of autonomous vehicles to drive coordinatedly according to a common centralized or decentralized decision-making strategy. The integration of onboard sensors and V2X communication also results in a solution that is more cost-effective than an approach based on high-quality sensors only.

The application of V2X communication to autonomous driving has been a research topic for many years, such as in the pioneering implementations of the PROMETHEUS initiative in Europe and the PATH Automated Highway System in the United States. More recently, several research activities [4, 5] and successful field trials of V2X communication for safety and traffic efficiency [6] have triggered manifold ongoing activities to bring V2X communication for autonomous driving closer to reality. Cooperative autonomous driving is currently being further developed by the European R&D projects AutoNet2030 [7], i-GAME,[1] AdaptIVe,[2] and COMPANION.[3]

We regard V2X communication in support of autonomous driving as a natural evolution of the communication system for cooperative vehi-

cles. The latter, here referred to as first generation V2X communication systems (1G-V2X), has been designed to provide driver assistance, which corresponds to level 1 in the definition of automation levels in SAE J3016 [8]. Higher levels of automation introduce new requirements that are not covered by 1G-V2X; therefore, the definition of new or enhanced messages, communication protocols, and their standardization is needed for cooperative autonomous driving.

The next section outlines some important use cases of autonomous driving where V2X communication plays a key role. The main V2X requirements for the implementation of the considered use cases are then identified, and an overview of the state-of-the-art V2X standards in Europe is given following that. Based on the presented requirements and standards, the message extensions required to support autonomous driving use cases are then explained. Finally, we conclude the article.

AUTONOMOUS DRIVING USE CASES

Use cases for autonomous driving can be grouped in three categories: close-distance, urban, and freeway use cases. Whereas close-distance use cases typically cover autonomous vehicles with the lowest operating velocities — an example is a vehicle able to park autonomously — urban and freeway use cases focus on common traffic situations. The latter two categories have the highest potential to improve traffic safety and efficiency. For this reason, we present the following four urban and freeway use cases for autonomous driving:

CONVOY DRIVING

One of the autonomous driving applications that has gained strong attention from research and industry in recent decades is platooning. In a platoon, vehicles in the same lane are grouped together in a stable formation with small inter-vehicle distances to increase road capacity, driver safety, and comfort. A platoon typically consists of one master, usually the leading vehicle, and multiple following vehicles.

However, a platoon is not the only approach to group vehicles on freeways. In a multi-lane convoy use case, as studied in the AutoNet2030 project, a master, centralized controller, or supervisor does not exist. Instead, the vehicle control, in both lateral and longitudinal directions, is distributed over all members of the convoy (Fig. 1). The result of this approach is that vehicle disturbances, such as a braking vehicle, affect all members of the convoy to a greater or lesser extent, resulting in a stable formation.

In order to maintain small inter-vehicle distances, convoy members rely on the high-frequency exchange of up-to-date and high-quality vehicle dynamics data among vehicles in the convoy. The convoy control algorithm presented in [9] requires just the vehicle dynamics information of neighbor vehicles, instead of the information of all convoy members. As such, the algorithm scales well to large convoys and converges easily to a desired formation when vehicles join and leave the convoy.

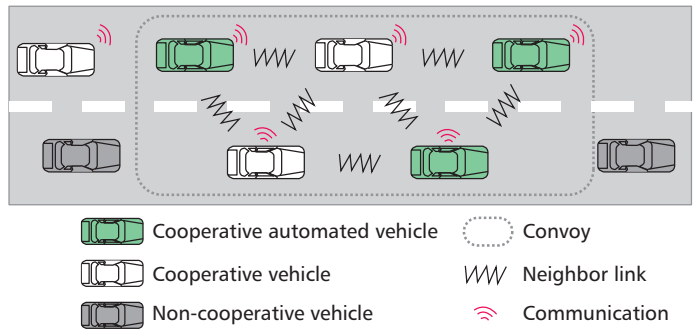

Figure 1. Exchange of vehicle dynamics data for multi-lane convoy driving.

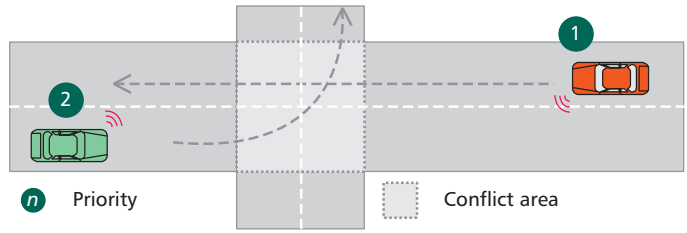

Figure 2. Priority-based coordination of incoming vehicles at an intersection with V2X communication.

COOPERATIVE LANE CHANGE

In the cooperative lane change use cases, cooperative vehicles (both autonomous and manually driven) collaborate to perform a lane change of one or a group of cooperative vehicles (e.g., a convoy) in a safe and efficient manner. Unlike in a traditional lane change situation, cooperative vehicles share their planned trajectories in order to negotiate and align their maneuvers.

The cooperative lane change may be aided by a roadside unit, which supports the communication among the interacting vehicles. However, when this infrastructure is not available, vehicles are forced to coordinate the lane change in an ad hoc fashion.

COOPERATIVE INTERSECTION MANAGEMENT

A cooperative intersection allows cooperative vehicles to traverse an intersection without the need for traffic lights [10]. This scenario requires a coordination mechanism in case their planned trajectories overlap.

A possible solution is shown in Fig. 2, where a roadside unit coordinates the traffic flow through the intersection by assigning relative priorities to incoming vehicles in real time. Then vehicles are able to cross the intersection efficiently following the order of their assigned priority.

COOPERATIVE SENSING

All of the above presented use cases, as well as autonomous driving in general, depend on an adequate and reliable perception of the vehicle surroundings in order to navigate through traffic and ensure safety with a high level of automation. Broken sensors, blind spots, and low level of trust in sensor data may degrade the perfor-

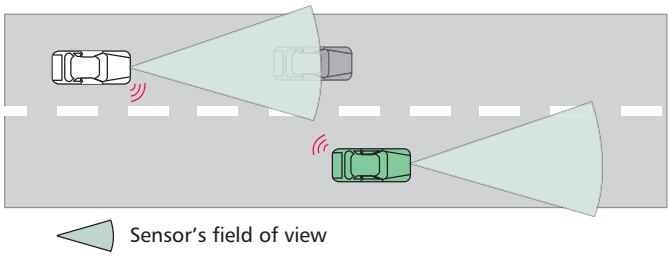

Figure 3. Exchange of detected objects for cooperative sensing.

mance or even disable automated functions of the vehicle.

In the cooperative sensing use case, shown in Fig. 3, neighbor vehicles share information gathered from local perception sensors in order to improve the quality and reliability of individual detections.

COMMUNICATION REQUIREMENTS

1G-V2X mainly addresses road safety and traffic efficiency for manually driven vehicles. Typical applications include obstacle warning, road works information, in-vehicle signage, traffic light phase assistance, and others [6]. The use cases for autonomous driving presented above demand new requirements. New *functional requirements* are below.

Additional Vehicle Status Data: In 1G-V2X, every vehicle broadcasts periodic safety messages to inform neighbors of its position, speed, heading, and other parameters. Autonomous vehicles need to include additional data in the periodic messages for the convoy driving and cooperative lane change use cases, such as their predicted path over the next few seconds.

Convoy Management: In 1G-V2X, a vehicle communicates with vehicles and roadside stations in its neighborhood, or located in a specific geographical region, also called a relevance area for safety information. Opposed to this "open group" concept without an explicit membership, a convoy represents a "closed group" where a vehicle needs to become a group member to participate. In order to create and maintain convoys, as well as to coordinate decentralized maneuvering negotiations, new fault-tolerant mechanisms for group management are needed.

Maneuver Negotiation: In autonomous driving, vehicles may actively need to reserve road space for lane change maneuvers. Unlike the distribution of periodic or event-driven safety messages for 1G-V2X, a reservation requires a negotiation among the involved vehicles to request and acknowledge the maneuver. This exchange enables optimal and safe trajectories for the cooperative vehicles and minimizes their collision risk.

Intersection Management: 1G-V2X is limited to the periodic broadcast of static and dynamic information of intersections, that is, to the distribution of the intersection topology and traffic light information, enabling use cases such as green light optimal speed advisory. It also allows requesting and changing the status of traffic light control systems for priority control and preemption of road traffic. With autonomous driving, communication for intersection management is extended to allow for more detailed information of the intersection geometry and to assign priorities to incoming vehicles, potentially displacing traffic lights.

Cooperative Sensing: Communication allows the exchange of locally acquired sensor data from the radar, camera, and other sensors. The captured data from the local sensors is aggregated into a list of detected objects along the road, such as obstacles, vehicles, and pedestrians, that can be exchanged with neighboring vehicles. Cooperative sensing increases the sensors' field of view to the V2X communication range and enables cooperative perception among vehicles. In 1G-V2X, the aggregation level of sensor data is much higher, and messages only carry a coarse event classifier and relevance area. Instead, the cooperative sensing use case requires the exchange of highly detailed information about the detected objects.

In addition to the functional requirements, specific qualitative *performance requirements* for cooperative autonomous driving include the following.

High Message Rate: In 1G-V2X, vehicles periodically broadcast safety messages with an interval between 100 ms and 1 s, where the rate within these limits is controlled by the dynamics of the generating vehicle and the load on the wireless channel. In contrast, the small inter-vehicle distance among autonomous vehicles requires the use of a high and fixed broadcast frequency with a timeliness guarantee on the information that autonomous vehicles possess about their neighbors. These requirements demand that autonomous vehicles have a complete and up-to-date environmental model, which allows them to coordinate maneuvers in a safe manner.

Data Load Control: The small inter-vehicle distance and corresponding high vehicle density lead to a higher data load in the network. This is even amplified by the high message rate and by additional data load for the exchange of control messages. In order to control the amount of data traffic in the network, efficient utilization of the available frequency spectrum, effective prioritization of messages by the decentralized congestion control (DCC) function, and strict control of the forwarding operations are required.

Low End-to-End Latency: The end-to-end latency is mainly composed of the delay to gather data from local sensors, the processing delay in the protocol stack, and the transmission delay over the wireless link. The end-to-end delay also includes the delay induced by the security mechanisms (generation and verification of signature and certificate, respectively) and by queuing delays in the DCC function. In 1G-V2X, the latency requirements for critical road safety applications are set to 300 ms (ETSI TS 102 539-1). In autonomous driving use cases such as convoy driving, the latency requirement is more stringent due to the smaller inter-vehicle distance between vehicles and also to ensure the string stability of large convoys.

Highly Reliable Packet Delivery: The requirement for reliable exchange of information is

more critical than in 1G-V2X, since a lost or erroneous message might cause a malfunction of the vehicle control algorithms and create a safety risk.

Both functional and performance requirements impose demanding challenges on the V2X communication system. This article proposes enhancements of 1G-V2X to meet some of these challenges.

CURRENT STANDARDS FOR V2X COMMUNICATION

The R&D efforts on V2X communication over the last years were accompanied by standardization efforts in the European Committee for Standardization (CEN), European Telecommunications Standards Institute (ETSI), IEEE, and International Standards Organization (ISO) in the context of cooperative intelligent transport systems (C-ITS). These activities have led to a consistent set of standards in Europe [11] and the United States [12]. We summarize the core standards for the European Release 1 defined by ETSI, which builds the basis for extensions for communication support toward autonomous vehicles, presented later in this article.[4]

The bottom layer of the reference model in Fig. 4 comprises access technologies: for V2X communication, ITS-G5[5] [EN 302 663] is the most relevant access technology in the context of this work. It has similar features as IEEE 802.11a (e.g., orthogonal frequency-division multiplexing, OFDM), but operates in the 5.9 GHz frequency band, enables a basic ad hoc mode, and disables management procedures. The medium access scheme relies on the well-known enhanced distributed channel access (EDCA) from IEEE 802.11 with carrier sense multiple access with collision avoidance (CSMA/CA) and quality of service (QoS) support. At the ITS network and transport layer, the GeoNetworking protocol (EN 302 636-4) provides single-hop and multihop packet delivery in an ad hoc network of vehicles and roadside stations. Specifically, it utilizes geographical positions carried in the packet headers for geographical addressing and forwarding of packets on the fly. On top of GeoNetworking, the Basic Transport Protocol, BTP (EN 302 636-5-1) provides a UDP-like connectionless transport protocol service.

Facilities layer standards specify application-supporting functionality: the cooperative awareness message (CAM) standard (EN 302 637-2) conveys critical vehicle state information in support of safety and traffic efficiency applications, with which receiving vehicles can track other vehicles' positions and movements. While the CAM is a periodic message sent over a single wireless hop, the decentralized environmental notification message (DENM) standard (EN 302 637-3) specifies a protocol for dissemination of event-driven safety information in a geographical region, typically via multiple wireless hops. Facility-layer messages for vehicle-to-infrastructure communication are specified in TS 103 301, including for transmission of static information about intersection topologies (MAP) and dynamic information for traffic lights. The standards

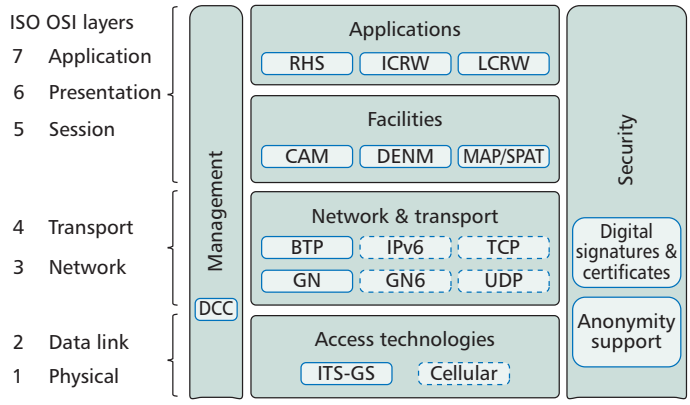

Figure 4. Reference model for 1G-V2X (functional components surrounded by solid lines are within the scope of this article).

at the application layer specify requirements for road hazard signaling (RHS), intersection collision risk warning (ICRW), and longitudinal collision risk warning (LCRW) (TS 101 539-1,-2,-3). RHS comprises use cases for initial deployment, including emergency vehicle approaching, hazardous location warning, and emergency electronic brake lights. ICRW and LCRW address potential vehicle collisions at intersections and rear-end/head-on collisions. Standards at the security block enable cryptographic protection by digital signatures and certificates (TS 103 097); changing pseudonyms for support of anonymity impedes tracking. Finally, management standards mainly cover support for decentralized data congestion control (TS 103 175).

MESSAGE EXTENSIONS FOR COOPERATIVE AUTONOMOUS DRIVING

The specification of the European 1G-V2X system and its corresponding standards have been driven by application requirements of RHS, ICRW, and LCRW. Cooperative autonomous driving creates additional communication requirements as described above and justifies a new generation of V2X communication. Compared to 1G-V2X, the new generation still relies on ITS-G5 but modifies the upper protocol layers. We extend and amend the facilities layer to satisfy the functional and performance requirements, in particular the CAM standard (ETSI EN 302 637-2), and we introduce new facilities layer components as shown in Fig. 5. The figure also illustrates enhanced networking and transport protocols; we have already shown that the GeoNetworking protocol can be adapted to meet the network requirements for platooning use cases [13]. Also, we introduce a modification of BTP called Reliable BTP (RBTP). However, here the focus is on facility layer components, indicated by solid boxes in Fig. 5.

The vehicle state information conveyed in a CAM (ETSI EN 302 637-2) is insufficient for the convoy and cooperative intersection use

[4] Available at http://etsi.org/standards

[5] ITS-G5 can be regarded as the European variant of the former "p"-amendment to IEEE 802.11, which has been integrated into IEEE 802.11-2012.

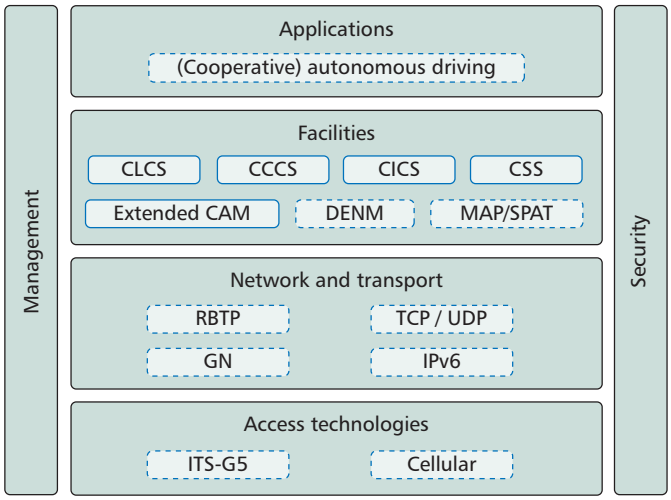

Figure 5. V2X communication architecture considered in the AutoNet2030 project.

cases. For planning maneuvers and avoiding safety-critical situations, both use cases require the exchange of periodic control-related data between neighbor vehicles, such as their predicted trajectory. This trajectory is calculated by the autonomous vehicle and cannot be measured with external sensors. Additionally, driving in a convoy requires the exchange of additional information, such as the distance to the preceding and following vehicles, target speed and acceleration, and convoy identifier.

In order to satisfy these data requirements, we propose to extend the CAM standard with additional *high* and *low* frequency containers that carry the control data specific to cooperative autonomous vehicles. The high frequency container includes only the minimum set of highly dynamic vehicle attributes for convoy driving to limit the total CAM size, including speed, heading, acceleration, and others. The low frequency container contains the less critical vehicle control data mentioned above.

In addition, two operating modes are introduced: *normal* mode and *high awareness* mode. In normal mode, CAMs are broadcast with variable frequency according to the standardized triggering conditions (i.e., between 1 and 10 Hz) depending on the vehicle dynamics. The high awareness mode augments the normal mode and increases the transmission frequency to a fixed value of 10 Hz. The newly introduced containers are only generated in high awareness mode and transmitted to single-hop neighbor vehicles using ITS-G5 on a separate service channel to relieve the heavily used control channel.

Convoy Control Communication Service

The *convoy control communication service* (CCCS) supports the exchange of information messages among cooperative vehicles in the convoy driving use case and satisfies the functional requirement for convoy management. The transmission frequency of convoy messages is dynamically adjusted depending on the convoy properties and traffic conditions. The messages exchanged among convoy vehicles via the CCCS enable each vehicle to maintain a local graph, whose nodes are the convoy members; the edges represent the dependence of the vehicle dynamics. A decentralized vehicle control algorithm performs the cooperative maneuvering, adjusting the vehicle lateral and longitudinal dynamics to keep a balanced formation and performing lane changes as required [9].

The message types offered by the CCCS to convoy members are the following.

Join/leave convoy: A join request is a single-hop broadcast message sent by an approaching vehicle, which detects a convoy and requests to become a convoy member. Similarly, a convoy vehicle that decides to abandon it (e.g., when it reaches its destination) will broadcast a leave request to inform its neighbors of its intention.

Lane change: A lane change message allows convoy vehicles to change their lane within the convoy. The message is broadcast by a convoy vehicle to inform its neighbors of a planned lane change. This way, the convoy members in the destination lane will adjust their positions to make space for the incoming vehicle.

Modify local graph: As a result of a lane change or a new vehicle entering the convoy, a vehicle may update its local graph. In this case, the new graph is broadcast to its neighbors by means of a modify local graph message. The neighbor vehicles then modify their own local graphs accordingly, thereby ensuring the consistency of the graphs among all the convoy members.

Cooperative Lane Change Service

The *cooperative lane change service* (CLCS) enables the communication for the cooperative lane change use case. CLCS supports maneuver negotiations among vehicles not belonging to the same convoy and relative space reservation by dedicated messages. The cooperative lane change is divided into three phases.

Search Phase: The planned lane change of a subject vehicle is announced in this phase, in search of a peer vehicle to start the lane change negotiation. This phase is optional and only executed when the subject vehicle has insufficient awareness of the traffic situation, and is unable to select the appropriate peer in advance. The planned lane change is described in a *lane change request* (LCR) message and is broadcast multihop around the lane change area. Any vehicle receiving the LCR will decide, based on its own planned trajectory, whether it is a suitable peer and will respond with a *lane change response*, which is unicast multihop to the subject vehicle. The subject vehicle eventually selects the most appropriate peer vehicle and informs all vehicles around the lane change area, including the selected peer vehicle, about this decision by broadcasting periodically an updated LCR message until the cooperative lane change has finished.

Preparation Phase: The selected peer vehicle opens the requested headway distance, and both vehicles adjust to the agreed speed and time of arrival. Once prepared, the peer vehicle informs

the subject vehicle with a *lane change prepared* message that the next phase can start.

Execution Phase: The lane change maneuver is executed in this phase without communication support of the CLCS component. The maneuver safety is ensured by the autonomous vehicles, based on received CAMs and local sensor information.

During all cooperative lane change phases, unexpected events may occur, which require to abort the lane change. In this case, a dedicated *lane change abort* (LCA) message is exchanged between the subject and peer vehicle. The CLCS component uses a retransmission and acknowledgment mechanism in order to improve the reliable delivery of LCA messages.

COOPERATIVE INTERSECTION CONTROL SERVICE

The *cooperative intersection control service* (CICS) supports the traversing of an intersection by cooperative autonomous vehicles, that is, *intersection management* as the functional requirement. In order to allow for a collision-free and deadlock-free intersection crossing, a roadside unit acts as intersection controller to coordinate the maneuvers of the vehicles approaching the intersection [10]. The intersection controller sends on-demand messages to incoming vehicles in order to assign them priorities based on information about their current status and desired trajectories; these regulate the order in which they are allowed to cross the intersection.

The message types offered by CICS are below.

Intersection Entry Request: This unicast message is sent by approaching vehicles, which detect the presence of the intersection controller. In the intersection entry request, the vehicle specifies its desired entry and exit lanes, the predicted time to enter the intersection, and information about the vehicle dynamics.

Intersection Entry Cancellation: With this message, a vehicle is able to inform the intersection controller that it wants to cancel a previous intersection entry request, for instance, in order to send a new entry request with different parameters.

Intersection Entry Status: The calculated relative priorities by the intersection controller are broadcast to all cooperative vehicles near the intersection. With this information, the vehicles are able to maneuver cooperatively and traverse the intersection safely.

It is worth noting that CICS also supports non-cooperative vehicles crossing the intersection. Two cases can be considered: first, if a non-cooperative vehicle is driving on its own, the intersection controller communicates the assigned priority by means of traffic lights; second, if the non-cooperative vehicle belongs to a platoon led by a cooperative vehicle, all the platoon vehicles will cross the intersection according to the priority assigned to the platoon leader.

COOPERATIVE SENSING SERVICE

The *cooperative sensing service* (CSS) enables the sharing of detected objects, including vehicles, pedestrians, cyclists, and so on, by means of *cooperative sensing messages* (CSMs) and enables the cooperative sensing use case.

A CSM can describe up to 16 detected objects in terms of their main attributes, including position, heading, speed, acceleration, and respective confidence level. Compared to raw sensor data, such as video frames of a camera or point cloud of a lidar, object attributes are less sensor-dependent and result overall in smaller messages being transmitted.

The tendency in the design of future autonomous vehicles is to combine the data of multiple sensors in order to create more concise detections and improve the overall detection accuracy compared to individual detections. The CSS component can interface with such a sensor fusion process in two ways: as a consumer and as a producer of perception data. As a consumer, the CSS constructs new CSMs with the sensor fusion output. As a producer, the CSS component can provide the content of received CSMs and act as a virtual sensor.

The nature of many perception sensors is to measure and provide relative object attributes, such as the distance or relative speed of a detected vehicle. Even though these values are appropriate for the control of an autonomous vehicle, relative object attributes are not suitable for inter-vehicle sharing. For this reason, the CSM only contains absolute object attributes.

The CSS component constructs CSMs at a rate of 1 Hz and disseminates the message over a single wireless hop to the neighbor vehicles. In order to deal with a higher data load, CSMs are transmitted on the service channel (e.g., SCH1) rather than on the control channel on which packets are typically transmitted in 1G-V2X.

CONCLUSION

Autonomous driving is regarded as a major innovative step that has the potential to fundamentally transform the mobility of people and goods. Today, most developments target standalone autonomous vehicles, which are capable of sensing the surroundings and control the vehicle based on this perception, with limited or no driver intervention. The inherent drawback of this solution is the lack of coordination among vehicles and the limited range of sensors, which results in suboptimal performance. Vehicle-to-vehicle/infrastructure communication (V2X) overcomes these drawbacks by increasing the planning horizon of autonomous vehicles and enabling two key features for autonomous driving: *cooperative maneuvering* and *cooperative sensing*.

In this article, we have presented four use cases for cooperative autonomous driving, and analyzed their requirements for safe and efficient operation. Compared to the first generation of V2X communication systems (1G-V2X) and its corresponding Release 1 of communication standards, cooperative autonomous driving requires adaptations and extensions. We have presented an evolution of the V2X communication system as standardized by ETSI. In particular, we have shown how the CAM standard as the V2X core facility can be extended, and we have introduced new facilities layer components.

The proposed V2X communication system for cooperative autonomous driving uses an enhanced ITS-G5-based protocol stack. This

Vehicle-to-vehicle/infrastructure communication (V2X) increases the planning horizon of autonomous vehicles and enables two key features for autonomous driving: cooperative maneuvering and cooperative sensing.

AutoNet2030 in particular will focus on the analysis of quantitative performance requirements using simulations and demonstration of AutoNet2030 concepts in a prototypical implementation. All in all, these developments will demonstrate the level of automation that can be achieved by V2X communication toward the vision of fully automated driving.

approach allows a gradual deployment of the next generation of V2X communication for cooperative autonomous driving relying on 1G-V2X. While the introduction of 1G-V2X is expected in the next few years, AutoNet2030 and other projects contribute to the development of concepts, protocols, prototype implementations, evaluation, and standards for the next generation of V2X communication systems. AutoNet2030 in particular will focus on the analysis of quantitative performance requirements using simulations and demonstration of AutoNet2030 concepts in a prototypical implementation. All in all, these developments will demonstrate the level of automation that can be achieved by V2X communication toward the vision of fully automated driving.

ACKNOWLEDGMENT

This work was supported by the European Commission under AutoNet2030, a collaborative project part of the Seventh Framework Programme for research, technological development and demonstration (Grant Agreement NO. 610542). The authors would like to thank all partners within AutoNet2030, and in particular Dr. Angelos Amditis (ICCS) as project coordinator, for their cooperation and valuable contribution.

REFERENCES

[1] S. Shladover, "Automated Vehicles for Highway Operations (Automated Highway Systems)," *Proc. Inst. Mechanical Engineers, Part I: J. Systems and Control Engineering*, vol. 219, 2005, pp. 53–75.
[2] C. Urmson *et al.*, "Autonomous Driving in Urban Environments: Boss and the Urban Challenge," *J. Field Robotics*, vol. 25, no. 8, 2008, pp. 425–66.
[3] J. Levinson *et al.*, "Towards Fully Autonomous Driving: Systems and Algorithms," *Proc. IEEE Intelligent Vehicles Symp.*, Baden-Baden, Germany, Jun. 2011, pp. 163–68.
[4] S. Kato *et al.*, "Vehicle Control Algorithms for Cooperative Driving with Automated Vehicles and Intervehicle Communications," *IEEE Trans. Intelligent Transportation Systems*, vol. 3, no. 3, Sept. 2002, pp. 155–61.
[5] J. Baber *et al.*, "Cooperative Autonomous Driving: Intelligent Vehicles Sharing City Roads," *IEEE Robotics Automation Mag.*, vol. 12, no. 1, Mar. 2005, pp. 44–49.
[6] H. Stübing *et al.*, "SIM-TD: A Car-to-X System Architecture for Field Operational Tests," *IEEE Commun. Mag.*, vol. 48, no. 5, 2010, pp. 148–54.
[7] A. de La Fortelle *et al.*, "Network of Automated Vehicles: The AutoNet 2030 Vision," *Proc. ITS World Congress*, Detroit, TX, Sept. 2014, http://www.autonet2030.eu.
[8] SAE, "Taxonomy and Definitions for Terms Related to On-Road Motor Vehicle Automated Driving Systems," *Soc. Automotive Engineers*, tech. rep. SAE J3016, Jan. 2014.
[9] A. Marjovi *et al.*, "Distributed Graph-Based Convoy Control for Networked Intelligent Vehicles," *Proc. IEEE Intelligent Vehicles Symp.*, Seoul, Korea, June 2015, pp. 138–43.
[10] X. Qian *et al.*, "Priority-Based Coordination of Autonomous and Legacy Vehicles at Intersection," *Proc. ITSC '14*, Qingdao, China, Oct. 2014.
[11] A. Festag, "Cooperative Intelligent Transport Systems (C-ITS) Standards in Europe," *IEEE Commun. Mag.*, vol. 12, no. 52, Dec. 2014, pp. 166–72.
[12] J. Kenney, "Dedicated Short-Range Communications (DSRC) Standards in the United States," *Proc. IEEE*, vol. 99, no. 7, July 2011, pp. 1162–82.
[13] I. Llatser, S. Kühlmorgen, A. Festag, and G. Fettweis, "Greedy Algorithms for Information Dissemination within Groups of Autonomous Vehicles," *Proc. IEEE Intelligent Vehicles Symp.*, Seoul, Korea, June 2015, pp. 1322–27.

BIOGRAPHIES

LAURENS HOBERT has been a development engineer since 2010 for the Automotive and Industry Laboratory of Hitachi Europe, Sophia Antipolis, France. He received his Diploma (M.Sc.) in telematics from the University of Twente in 2012. His research interests include intelligent transport systems, wireless communication, automated driving, and software prototyping. He has been involved in various European projects, including CoVeL, DRIVE-C2X, eCo-FEV, and AutoNet2030, and actively contributes to standardization in ETSI Technical Committee ITS and the CAR-2-CAR Communication Consortium.

ANDREAS FESTAG is research group leader and lecturer at the Technical University Dresden, Vodafone Chair Mobile Communication Systems. He received a diploma degree (1996) and Ph.D. (2003) in electrical engineering from the Technical University of Berlin. His research is concerned with 5G cellular systems and vehicular communication. He actively contributes to the CAR-2-CAR Communication Consortium and ETSI Technical Committee ITS.

IGNACIO LLATSER received a double degree in telecommunication engineering and computer science (2008), a Master's degree (2011), and a Ph.D. degree (2014) from the Technical University of Catalonia, Barcelona, Spain. He is currently a postdoctoral researcher at the Technical University of Dresden, Germany, in the framework of the FP7 project AutoNet2030. His research interests lie in the fields of nanoscale communication networks, vehicular networks, and autonomous driving.

LUCIANO ALTOMARE is a researcher and developer at Centro Ricerche Fiat, FCA company, since 2007. He received a Master's degree (2006) in physics from the University of Bologna, Italy. Currently his research activity is mainly focused on vehicle-to-vehicle applications and prototype integration.

FILIPPO VISINTAINER graduated in physics and is a senior researcher of Centro Ricerche FIAT, Trento Branch, part of FCA Vehicle Research and Innovation, where he has been working since 2001. Within the European Framework Programmes he has been Project Manager within several projects on intelligent mobility, preventive safety, e-Inclusion, and vehicular communication, including DRIVE C2X, TEAM IP, AutoNet2030, and AdaptIVe. Lately he has been leading an innovation project of his company on connected vehicle services.

ANDRAS KOVACS has been working in the field of ITS for 10 years. His background is in telecommunication networks research. He has contributed to the work of the Car-2-Car Communication Consortium in the past, and currently participates in the work of ETSI ITS. His research interests relate to geonetworking, ITS applications, and their testing aspects. He is currently the director of R&D at BroadBit and the technology manager of AutoNet2030.

IEEE INTERNATIONAL CONFERENCE ON COMMUNICATIONS
IEEE ICC PARIS 21-25 MAY 2017

IEEE International Conference on Communications
21-25 MAY 2017 // PARIS, FRANCE
Bridging People, Communities, and Cultures

IEEE
IEEE ComSoc
IEEE Communications Society

CALL FOR PAPERS AND PROPOSALS

IEEE ICC 2017 will be held at Palais des Congrès - Porte Maillot, Paris, France, 21-25 May 2017. Located in the heart of the City of Lights, IEEE ICC 2017 will exhibit an exciting technical program, complete with 13 Symposia highlighting recent progress in all major areas of communications. IEEE ICC 2017 will also feature high-quality Tutorials and Workshops, Industry Panels and Exhibitions, as well as Keynotes from prominent research and industry leaders.

Prospective authors are invited to submit high-quality original technical contributions for presentation at the conference and publication in the IEEE ICC 2017 Proceedings and IEEE Xplore. Proposals for Tutorials, Workshops, and Forums are also invited. Visit http://icc2017.ieee-icc.org for more details.

TECHNICAL SYMPOSIA

SELECTED AREAS IN COMMUNICATIONS

Access Systems and Networks
Steven Hranilovic,
McMaster University, Hamilton, Canada

Big Data Networking
Shui Yu, Deakin University, Australia

Cloud Communications and Networking
Ioannis Papapanagiotou,
Purdue University, USA

Communications for the Smart Grid
Deepa Kundur, University of Toronto, Canada

Data Storage
Onur Ozan Koyluoglu,
University of Arizona, USA

E-Health
Jaime Lloret Mauri,
Polytechnic University of Valencia, Spain

Internet of Things
Antonio Jara,
University of Applied Sciences Western Switzerland (HES-SO), Switzerland

Molecular, Biological, and Multi-Scale Communications
Urbashi Mitra, University of Southern California, USA

Satellite and Space Communications
Igor Bisio, University of Genoa, Italy

Social Networking
Damla Turgut, University of Central Florida, USA

Software Defined Networking & Network Function Virtualization
Latif Ladid, Luxembourg University, Luxembourg

Ad-Hoc and Sensor Networking
Shibo He, Zhejiang University, China
Adlen Ksentini,
University of Rennes, France
Cheng Li,
Memorial University of Newfoundland, Canada
Azzedine Boukerche,
University of Ottawa, Canada
Davide Dardari,
University of Bologna, Italy
Hämäläinen Jyri,
Aalto University, Finland
Yahong Rosa Zheng,
Missouri University of Science and Technology, USA

Cognitive Radio and Networks
Oliver Holland, King's College London, UK
Walid Saad, Virginia Tech, USA

Communication and Information Systems Security
Peter Mueller, IBM, Switzerland
Cong Wang, University of Hong Kong, China

Communications Software, Services and Multimedia Applications
Maria G. Martini, Kingston University London, UK
Said Hoceini, University of Paris12, France
Abdallah Shami, Western University, Canada

Communication Theory
Ender Ayanoglu,
University of California, Irvine, USA
Fulvio Babich, University of Trieste, Italy
Steven Weber, Drexel University, USA

Green Communications Systems and Networks
Cicek Cavdar,
Royal Institute of Technology Stockholm, Sweden
Michela Meo, Politecnico di Torino, Italy

Communications QoS, Reliability and Modeling
Dzimitry Kliazovich,
Luxembourg University, Luxembourg
Sami Souihi, UPEC, France
Kohei Shiomoto, NTT, Japan

Next Generation Networking and Internet
Shiwen Mao, Auburn University, USA
Mahesh K. Marina, University of Edinburgh, UK
Sidi-Mohammed Senouci,
University of Bourgogne, France

Signal Processing for Communications
Michael Buehrer, Virginia Tech, USA
Tomohiko Taniguchi,
Fujitsu Laboratories Limited, Japan

Optical Networks and Systems
Grzegorz Danilewicz,
Poznan University of Technology, Poland
George Rouskas,
North Carolina State University, Raleigh, USA

Wireless Communications
Mohamad Assaad,
CentraleSupelec, France

Mobile and Wireless Networking
Mohammed Atiquzzaman,
University of Oklahoma, USA
Mehdi Bennis,
University of Oulu, Finland
Jalel Ben-Othman,
University of Paris 13, France
Shaowei Wang,
Nanjing University, China

INDUSTRY FORUMS AND EXHIBITION PROGRAM
IEEE ICC 2017 will feature several prominent keynote speakers, major business and technology forums, and a large number of vendor exhibits. Submit your proposals to the IF&E Co-Chairs Luis M. Correia (luis.correia@inov.pt) and Jamshid Khun-Jush (khunjush@qti.qualcomm.com).

TUTORIALS
Proposals are invited for half- or full-day tutorials in all communication and networking topics. For enquiries, please contact the Tutorials Program Co-Chairs Hanna Bogucka (hanna.bogucka@put.poznan.pl) and Luc Vandendorpe (luc.vandendorpe@uclouvain.be).

WORKSHOPS
Proposals are invited for half- or full-day workshops in all communication and networking topics. For enquiries, please contact the Workshops Program Co-Chairs Abbas Jamalipour (a.jamalipour@ieee.org) and Constantinos Papadias (cpap@ait.gr).

2017 COMMITTEE

General Chair
Jean-Luc Beylat, Nokia, France

Executive Chair
Hikmet Sari, CentraleSupelec, France

Technical Program Co-Chairs
Merouane Debbah, Huawei, France
David Gesbert, EURECOM, France

Technical Program Symposia Chair
Abdelhamid Mellouk,
University of Paris-Est Creteil VdM (UPEC), France

Industry Forums & Exhibition Co-Chairs
Luis M. Correia,
IST - University of Lisbon, Portugal
Jamshid Khun-Jush,
Qualcomm, Germany

Tutorials Program Co-Chairs
Hanna Bogucka,
Poznan University of Technology, Poland
Luc Vandendorpe,
Catholic University of Louvain, Belgium

Workshops Program Co-Chairs
Abbas Jamalipour,
University of Sydney, Australia
Constantinos Papadias,
Athens Information Technology, Greece

IMPORTANT DATES

Paper Submission: 28 October 2016

Tutorial Proposals: 11 November 2016

IF&E Proposals: 11 November 2016

Workshop Proposals: 24 June 2016

Paper Acceptance Notification: 27 January 2017

Camera-Ready Papers Due: 24 February 2017

Full details of submission procedures are available at icc2017.ieee-icc.org

#IEEEICC17

Guidelines for our Authors

Format of the manuscripts

Original manuscripts and final versions of papers should be submitted in IEEE format according to the formatting instructions available on
http://www.ieee.org/publications_standards/publications/authors/authors_journals.html#sect2,
"Template and Instructions on How to Create Your Paper".

Length of the manuscripts

The length of papers in the aforementioned format should be 6-8 journal pages.
Wherever appropriate, include 1-2 figures or tables per journal page.

Paper structure

Papers should follow the standard structure, consisting of *Introduction* (the part of paper numbered by "1"), and *Conclusion* (the last numbered part) and several *Sections* in between.
The Introduction should introduce the topic, tell why the subject of the paper is important, summarize the state of the art with references to existing works and underline the main innovative results of the paper. The Introduction should conclude with outlining the structure of the paper.

Accompanying parts

Papers should be accompanied by an *Abstract* and a few *index terms (Keywords)*. For the final version of accepted papers, please send the *short cvs* and *photos* of the authors as well.

Authors

In the title of the paper, authors are listed in the order given in the submitted manuscript. Their full affiliations and e-mail addresses will be given in a footnote on the first page as shown in the template. No degrees or other titles of the authors are given. Memberships of IEEE, HTE and other professional societies will be indicated so please supply this information. When submitting the manuscript, one of the authors should be indicated as corresponding author providing his/her postal address, fax number and telephone number for eventual correspondence and communication with the Editorial Board.

References

References should be listed at the end of the paper in the IEEE format, see below:

a) Last name of author or authors and first name or initials, or name of organization
b) Title of article in quotation marks
c) Title of periodical in full and set in italics
d) Volume, number, and, if available, part
e) First and last pages of article
f) Date of issue

[11] Boggs, S.A. and Fujimoto, N., "Techniques and instrumentation for measurement of transients in gas-insulated switchgear," IEEE Transactions on Electrical Installation, vol. ET-19, no. 2, pp.87–92, April 1984.

Format of a book reference:

[26] Peck, R.B., Hanson, W.E., and Thornburn, T.H., Foundation Engineering, 2nd ed. New York: McGraw-Hill, 1972, pp.230–292.

All references should be referred by the corresponding numbers in the text.

Figures

Figures should be black-and-white, clear, and drawn by the authors. Do not use figures or pictures downloaded from the Internet. Figures and pictures should be submitted also as separate files. Captions are obligatory. Within the text, references should be made by figure numbers, e.g. "see Fig. 2."
When using figures from other printed materials, exact references and note on copyright should be included. Obtaining the copyright is the responsibility of authors.

Contact address

Authors are requested to send their manuscripts via electronic mail or on an electronic medium such as a CD by mail to the Editor-in-Chief:

Rolland Vida
Department of Telecommunications and Media Informatics
Budapest University of Technology and Economics
2 Magyar Tudósok krt.
Budapest, 1117 Hungary
vida@tmit.bme.hu

IEEE EUROCON 2017

6 – 8 July 2017 Ohrid, Republic of Macedonia

Important Dates

28 November 2016
Full paper submission
1 February 2017
Paper acceptance notification
6 April 2017
Early registration, Camera-ready papers
30 September 2016
Special Session proposal deadline

Honorary Chair

Karen Bartleson
2017 IEEE President

General Chair

Ljupco Karadzinov, IEEE Rep. of Macedonia Section Chair
chair@eurocon2017.org

The conference includes a student competition and the **EUROCON 2017 Best Student Paper Award:**
Tablet computer

IEEE R8 Best Student Paper Contest 2017 awards will be presented at the conference

Early Registration Fees

IEEE Member	370 €
IEEE Student Member	280 €
IEEE Life Member	280 €
Non IEEE members	450 €
Students non member	330 €
Accompanying person	260 €

Lunches included

Second Call for Papers (Sep 2016)

IEEE EUROCON 2017 – 17th IEEE International Conference on Smart Technologies

EUROCON is a flagship event of the IEEE Region 8 (Europe, Middle East and Africa) held every two years in a different country with participants from all over the world. EUROCON is a major international forum for the exchange of ideas, theory basics, design methodologies, techniques and experimental results between academia, research institutions and practitioners from industry. It has achieved a considerable success during the past 16 editions in all fields of electrical and electronic engineering, ICT and computer science covered by all IEEE Societies. The technical sessions are grouped in **four tracks**:

- Information & Communication Technologies
- Circuits, Systems and Signal Processing
- Power Engineering and Energy
- Industrial and Consumer Applications

KEYNOTE PLENARY LECTURES

5G as an Enabler of New Energy, Transport, Production and other Verticals by Professor Petar Popovski, IEEE Fellow, Wireless Communications, Department of Electronic Systems, Aalborg University, Denmark

Data Science Profession and Education by Professor Yuri Demchenko, System and Network Engineering Research Group, University of Amsterdam, Netherlands

Digital Life Live by Dr. Andrej Vckovski, CEO and co-founded of Netcetera, President of the Swiss Internet Industry Association, Zürich, Switzerland

5G Mobile Networks: Implications for Operators, Verticals and End Users by Professor Eckhard Grass, Leader of Joint-Lab Wireless Broadband Communication Systems (IHP - HUB), IHP - Leibniz-Institut für innovative Mikroelektronik and Humboldt-Universität zu Berlin, Germany

State of the Art in Nanotechnology by Professor Stephen Goodnick, IEEE Fellow, Department of Electrical Engineering, Ira A. Fulton School of Engineering, Arizona State University, USA

Does DC Distribution Make Sense? by Josep M. Guerrero Professor in Microgrid, IEEE Fellow, Department of Energy Technology, Aalborg, Denmark.

What does European Energy Turnover (Energiewende) Mean for Small countries by Professor Rafael Mihalič, Head of the Department of Power Systems and Devices, University of Ljubljana, Slovenia

The conference venue is the hotel complex Metropol Lake Resort, located near the magnificent city of Ohrid in the Republic of Macedonia. The resort is located about 7 km south from the city of Ohrid and 14 km from the Ohrid airport. The distance from Skopje airport is approximately 200 km and 175 km from Skopje city centre. The Resort enjoys a picturesque location on the coast of Lake Ohrid in the downhill of the mountain Galichica, boasting 500 m long private beach with swimming pools and playgrounds, its own port, landscaped gardens and pinewoods, and fantastic views overlooking the lake and surrounding National Park Galichica. The Ohrid city is referred to as the "Jerusalem of the Balkans" due to its richness in churches, picturesque sites and monuments, while the Ohrid Lake, as the oldest in Europe, has unique flora and fauna with more than 200 endemic species. Both, the city and the lake, are protected as UNESCO Cultural and Natural World Heritage and are regarded as one of the best summer destinations.

Web page: http://eurocon2017.org/

SCIENTIFIC ASSOCIATION FOR INFOCOMMUNICATIONS

Who we are

Founded in 1949, the Scientific Association for Infocommunications (formerly known as Scientific Society for Telecommunications) is a voluntary and autonomous professional society of engineers and economists, researchers and businessmen, managers and educational, regulatory and other professionals working in the fields of telecommunications, broadcasting, electronics, information and media technologies in Hungary.

Besides its 1000 individual members, the Scientific Association for Infocommunications (in Hungarian: Híradástechnikai Tudományos Egyesület, HTE) has more than 60 corporate members as well. Among them there are large companies and small-and-medium enterprises with industrial, trade, service-providing, research and development activities, as well as educational institutions and research centers.

HTE is a Sister Society of the Institute of Electrical and Electronics Engineers, Inc. (IEEE) and the IEEE Communications Society.

What we do

HTE has a broad range of activities that aim to promote the convergence of information and communication technologies and the deployment of synergic applications and services, to broaden the knowledge and skills of our members, to facilitate the exchange of ideas and experiences, as well as to integrate and harmonize the professional opinions and standpoints derived from various group interests and market dynamics.

To achieve these goals, we…

- contribute to the analysis of technical, economic, and social questions related to our field of competence, and forward the synthesized opinion of our experts to scientific, legislative, industrial and educational organizations and institutions;
- follow the national and international trends and results related to our field of competence, foster the professional and business relations between foreign and Hungarian companies and institutes;
- organize an extensive range of lectures, seminars, debates, conferences, exhibitions, company presentations, and club events in order to transfer and deploy scientific, technical and economic knowledge and skills;
- promote professional secondary and higher education and take active part in the development of professional education, teaching and training;
- establish and maintain relations with other domestic and foreign fellow associations, IEEE sister societies;
- award prizes for outstanding scientific, educational, managerial, commercial and/or societal activities and achievements in the fields of infocommunication.

Contact information

President: **GÁBOR MAGYAR, PhD** • *elnok@hte.hu*

Secretary-General: **ISTVÁN BARTOLITS** • *bartolits@nmhh.hu*

Operations Director: **PÉTER NAGY** • *nagy.peter@hte.hu*

International Affairs: **ROLLAND VIDA, PhD** • *vida@tmit.bme.hu*

Address: H-1051 Budapest, Bajcsy-Zsilinszky str. 12, HUNGARY, Room: 502

Phone: +36 1 353 1027

E-mail: *info@hte.hu*, Web: *www.hte.hu*